Taylor & Francis
Taylor & Francis Group

Critical Insights in Climate Change

ISSN: 2993-1495 (Online) Journal homepage: www.tandfonline.com/journals/tclc20

Competing effects of sea ice change control the pace and amplitude of millennial-scale climate oscillations

Brooke Snoll, Ruza Ivanovic , Lauren J. Gregoire , Sam Sherriff-Tadano & Yvan Romé

To cite this article: Brooke Snoll, Ruza Ivanovic , Lauren J. Gregoire , Sam Sherriff-Tadano & Yvan Romé (2025) Competing effects of sea ice change control the pace and amplitude of millennial-scale climate oscillations, Critical Insights in Climate Change, 1:1, 2557072, DOI: 10.1080/29931495.2025.2557072

To link to this article: https://doi.org/10.1080/29931495.2025.2557072

RESEARCH ARTICLE

CRITICAL INSIGHTS IN CLIMATE CHANGE
2025, VOL. 1, NO. 1, 2557072
https://doi.org/10.1080/29931495.2025.2557072

OPEN ACCESS Check for updates

Competing effects of sea ice change control the pace and amplitude of millennial-scale climate oscillations

Brooke Snoll[a], Ruza Ivanovic[a], Lauren J. Gregoire[a], Sam Sherriff-Tadano[b] and Yvan Romé[a]

[a]School of Earth and Environment, University of Leeds, Leeds, UK; [b]Department of Physics and Earth Sciences, University of the Ryukyus, Nishihara, Okinawa Prefecture, Japan

ARTICLE HISTORY Received 20 December 2024; Revised 4 August 2025; Accepted 13 August 2025

Cite as: Critical Insights in Climate Change, 1, 2025, doi: 10.1080/29931495.2025.2557072

ABSTRACT

Despite an increasing number of climate simulations showing millennial-scale oscillatory regimes, such as Dansgaard-Oeschger cycles, the mechanisms behind past abrupt climate changes remain elusive. Based on previous experiments that simulated such variability under Last Glacial Maximum boundary conditions forced with fixed freshwater snapshots derived from the early last deglaciation ice sheet history, this papers investigates the Atlantic Meridional Overturning Circulation (AMOC) oscillatory mechanisms under different climate forcings (i.e., different levels of CO_2 concentrations and varying orbital parameters). Our results show that sea ice plays a key role as a pacer, regulating AMOC transitions between strong/interstadial and weak/stadial modes. At lower CO_2 levels sea-ice volume increases and the warm-mode duration is reduced through enhanced summer sea ice melt. In contrast, higher levels of CO_2 lead to thinner sea ice and, in turn, cooler North Atlantic subsurface temperatures and suppressed oscillations. Orbital changes influence seasonality and localized sea ice dynamics, shortening or lengthening strong AMOC periods based on obliquity variations. These simulations, performed with the HadCM3 general circulation model, show that small climate changes can impact the existence and shape of oscillations in glacial climates, potentially explaining the variability in the periodicity and amplitude of Dansgaard-Oeschger cycles and transitions from weak to strong AMOC states.

KEYWORDS Millennial-scale variability; AMOC; general circulation model; convection–advection oscillator; climatic controls

CRITICAL INSIGHTS SUMMARY

Sea Ice as the Silent Metronome of Abrupt Climate Change

Sea ice, long considered a passive responder, may in fact set the rhythm of Earth's most dramatic climate shifts. New simulations show how subtle shifts in sea ice cover can accelerate, dampen, or even prevent millennial-scale oscillations—such as Dansgaard-Oeschger cycles that punctuated the last ice age.

At the heart of these abrupt swings lies the Atlantic Meridional Overturning Circulation (AMOC), whose strength determines how heat is distributed across the North Atlantic. By tweaking levels of atmospheric carbon dioxide (CO_2) and Earth's orbital configuration in a general circulation model, this study reveals that sea ice controls whether the AMOC pulses between weak and strong modes, or locks into stability. Lower CO_2 fuels thicker ice, shortening warm phases through increased melt, while higher CO_2 thins ice and suppresses oscillations. Likewise, orbital shifts alter seasonality, reshaping the timing and intensity of these transitions.

These findings suggest that the climate's "window of opportunity" for instability is narrower—and more sensitive to background conditions—than previously thought. The interplay of ice, salt, and circulation creates a delicate balance where even minor changes can tip the system toward stability or chaos.

For researchers, this work sharpens the mechanistic link between sea ice and abrupt climate variability, offering a framework to interpret paleoclimate records. Looking forward, it hints that future ice loss in a warming world could suppress natural oscillatory modes but amplify the risk of abrupt, irreversible AMOC shifts. In 5–10 years, such insights may underpin new climate risk assessments, bridging glacial histories with projections of future ocean tipping points.

CONTACT Brooke Snoll ee19b2s@leeds.ac.uk, b.snoll@leeds.ac.uk

Supplemental data for this article can be accessed online at https://doi.org/10.1080/29931495.2025.2557072.

1. Introduction

With increasing concern about a tipping point in the AMOC linked to the unprecedented rate of increase in atmospheric carbon dioxide [1], we can look to past abrupt climate changes to gain a better understanding of these potential ocean processes. During the Last Glacial period (~115 to 11.7 thousand years ago [ka BP]), millennial-scale variability in the form of rapid climate transitions between warm and cold regimes was observed in surface air temperature proxy records of Greenland but also experienced worldwide (e.g., [2–4]). These abrupt climate changes, referred to as Dansgaard-Oeschger (D-O) cycles, were transitions of up to 10–15 °C in Greenland [5–7]. D-O cycles are best documented during Marine Isotope Stage 3 (MIS3; between 60 and 25 ka BP [8]), where they can be observed in Greenland ice cores [9–11] and more globally in proxy records of the Tropics [12,13], North and South America [13–16], and Eurasia [17,18]. There were ~25 occurrences of D-O cycles during the Last Glacial Period, with a periodicity of ~1500 years [19,20].

Despite decades of research on D-O cycles, uncertainty remains as to the underpinning mechanisms and drivers of these transitions. There is, however, a large consensus that the AMOC plays a critical role in the climate transitions (e.g., [21–26]). The strength and structure of the AMOC is a key control on the North Atlantic and Arctic climate. When the AMOC is strong (weak), more (less) Atlantic heat is transported northward, causing regional warming (cooling) in the North Atlantic and surrounding land masses [19]. AMOC strength is dependent on the stratification of the North Atlantic main convection site's water column (i.e., the Labrador Sea, Irminger Sea, and the Greenland, Iceland, and Norwegian seas (or GIN seas) [27,28]).

Previous studies have shown that the AMOC responds to freshwater input into the North Atlantic from melting icebergs and ice sheets; for example, if freshwater is discharged into the critical sites of ocean convection, the circulation strength can be disrupted (e.g., [29–36]). Iceberg discharge can release large amounts of freshwater into these regions during Heinrich events (e.g., [37]), but the timing of such events does not match the records of abrupt AMOC weakening [38,39]. Instead, the freshwater source necessary to trigger AMOC tipping points may have come from the background melt of the ice sheets of the Last Glacial Period [40] while the iceberg discharge provided a feedback mechanism to sustain the weak AMOC mode [41].

The impact of ice sheet melt on the climate has been investigated by multiple studies (e.g., [33,41–43]). However, the sensitivity of abrupt climate changes in the North Atlantic Ocean to changes in freshwater fluxes and atmospheric climate forcings [44–49] needs to be further constrained to find the cause behind abrupt climate changes in the Quaternary. Climate modeling groups have investigated what conditions are required for oscillatory behavior in the AMOC in their respective models. This initiative has become more and more successful in recent years (e.g., [50,51], and experiments referenced by [23]) under a wide range of parameter values, boundary conditions, and forcings, including pre-industrial or present-day conditions (e.g., [52–54]), glacial (Last Glacial Maximum) conditions (e.g., [50,55,56]) and MIS3 conditions (e.g., [57,58]). Background climate and initial ocean state are thought to be important for how responsive ocean circulation is to a meltwater flux (e.g., whether AMOC is already strong and deep or weak and shallow [59–62]); therefore, the choice of a model's boundary conditions in the palaeo setting (e.g., ice sheet geometry, atmospheric trace gas concentrations, or orbital parameters) can influence the ocean's sensitivity to freshwater perturbation [55,58,63].

Barker and Knorr [64] infer from geological records that some combinations of background conditions (trace gases, orbital forcing, ice sheet geometries, ocean gateways, etc.) create optimal environments for triggering millennial-scale climate variability, affecting their frequency and/or amplitude. More specifically, such conditions are thought to exist when both ice volume and atmospheric CO_2 concentrations are at levels midway between full glacial and warm interglacial. When the background climate is mid-glacial, CO_2 concentrations are not high enough to make the AMOC monostable and strong [53,65,66], and the ice sheets are not so large that they make the AMOC monostable and weak [66]. The region in the parameter space where the AMOC is multi-stable is called the "window of opportunity." The climate system may have entered such a "window of opportunity" at MIS3, facilitating the establishment of D-O cycles, or may have moved through a "window of opportunity" during periods of deglaciation, when ice sheets are melting away and atmospheric CO_2 is rising [64]. This "window of opportunity" can also move with respect to one variable—e.g., CO_2—with dependence on another—e.g., ice sheet meltwater [67].

Multiple modeling groups have tested the impact of atmospheric CO_2 and orbital forcings over the course of the Last Glacial Period on the occurrence of abrupt climate changes. Climate simulations indicate that oscillations often occur within a narrow range of CO_2 concentrations (between 185 and 230 ppm [53,57,63,68]), matching the range under which D-O cycles occurred during MIS3. In addition, changes in Earth's orbit are known to drive glacial terminations throughout at least the last 800,000 years [69,70]. Multiple studies have demonstrated that changes in orbital configuration (more specifically obliquity and precession) can impact millennial-scale climate variability [55,58,71,72] and the

periodicity of oscillations [29,55], with stronger boreal seasonality being shown to lead to shorter periodicity.

Climate models are useful for validating the existence of a "window of opportunity" hypothesis, although its location in the parameter space may be model dependent. For example, where Klockmann et al. [53] cannot produce climate oscillations under glacial ice sheet layout, Peltier and Vettoretti [56] can with Last Glacial Maximum ice sheets. The oscillations presented by [50] are triggered by meltwater fluxes, whereas Kuniyoshi et al. [55] do not use freshwater forcing to obtain their oscillations. There are instances of quasi-consistency between models—for example, where oscillatory behavior occurs within a similar range of atmospheric CO_2 concentration—although other boundary and background climate conditions are significantly different [68]. However, across models and climate experiments, the characteristics of stadial–interstadial climate oscillations vary considerably (see simulations listed by [23]). Not only do simulated oscillations not always have comparable amplitudes and periodicities, it is also uncertain whether they are even governed by the same mechanism; as highlighted by [23], the precise controls on the oscillations are hard to identify.

More than simply exploring the "window of opportunity," models can be used to understand the underlying mechanisms that explain why a specific climate state is more or less susceptible to abrupt change, which may have broader significance beyond the specific model structure and inputs. Previous mechanistic studies have focused on the role of the AMOC and the impact of changes in temperature and salinity on deep water formation sites' stratification and activity. Li et al. [73], Dokken et al. [74], Vettoretti and Peltier [26], Li and Born [75], and Sadatzki et al. [76], for example, demonstrate the control of sea ice in the GIN seas on the transition between cold and warm phases. Vettoretti and Peltier [26] show with Last Glacial Maximum simulations that Arctic and North Atlantic sea ice governs the duration of the warm and cold regimes. Advection of sea ice into AMOC convection sites in the North Atlantic increases stratification and forces an end to the warm regime, whereas the cold regime is terminated by ocean heat loss in the same region. When in a cold regime, sea ice concentration increases, insulating the surface ocean. Eventually, this leads to the warmer waters melting the sea ice above it, starting the transition to interstadial conditions [26,74]. Other research groups have looked deeper into the control of sea ice on salinity in oscillations (e.g. [56,57,77]). Armstrong et al. [57] demonstrate how the seasonal nature of sea ice can impact the salinity content of the subpolar gyre. During the warm regime, freshening is reduced in the subpolar gyre, increasing salinity, whereas during the cold regime, sea ice freshening dominates in the region, weakening convection. While hypotheses are emerging on the mechanisms causing AMOC oscillations and abrupt changes, there is not yet an understanding of how D-O mechanisms are influenced by orbital and CO_2 forcings.

In this study, we investigate how and why the characteristics of the climate oscillations simulated by [50] (henceforth referred to as *Romé22*) are affected by different greenhouse gas concentrations and orbital configurations. These simulations come from one of the few studies, to our knowledge, that have successfully modeled AMOC oscillations under Last Glacial Maximum climate conditions [50,55,56,63]. *Romé22* follow the Paleoclimate Modelling Intercomparison Project phase 4 (PMIP4) Last Glacial Maximum experimental design (including 21 ka BP orbit, 190 ppm atmospheric pCO_2 [78]) with the GLAC-1D ice sheet reconstruction [79–82] and associated boundary conditions. Crucially, on top of the PMIP4 protocol, the simulations include fixed patterns and amplitudes of meltwater inputs, derived from the early deglacial GLAC-1D meltwater history. Some of those meltwater scenarios, which are constant in time, cause millennial-scale oscillations between strong and nearly or completely collapsed AMOC modes. Greenland surface temperatures cool and warm by ~10 °C with a periodicity of about 1,500 years. Romé et al. [83] identify a precise mechanism for the *Romé22* oscillatory behavior. The so-called convection–advection oscillator hypothesis incorporates fast North Atlantic ocean buoyancy changes as the convection component and slow reorganization of global salinity as the advection component. We explore how changes in climate forcings affect the dynamics of D-O cycles.

We test how the convection–advection mechanism is affected by perturbations in the background CO_2 and orbit, by selecting one of the oscillating simulations from *Romé22* and altering atmospheric CO_2 concentration and orbital configuration. We present the results of the CO_2 and orbit changes and the corresponding impact on the convection–advection mechanism (Sections 3.2 and 3.3). We discuss the implications on AMOC stability (Section 4.1) and relevance to glacial termination (Section 4.2).

2. Methods

2.1. Model description

We used the Hadley Centre Coupled Model version 3 (HadCM3), a coupled ocean–atmosphere–vegetation general circulation model [84,85] with minor modifications described by [86]. HadCM3 has an atmospheric resolution of 2.5° latitude by 3.75° longitude with 19 vertical levels starting at the surface and ending at 10 hPa. The ocean's horizontal resolution is 1.25° by 1.25° with 20 vertical layers from the surface of the ocean to ~5500 m deep, with maximum resolution at the surface. The ocean volume stays constant throughout the simulations.

Vegetation is represented by the dynamic vegetation model TRIFFID (Top-down Representation of Interactive Foliage and Flora Including Dynamics) coupled to the atmospheric general circulation model and linked to the land surface with MOSES 2.1 (or the Met Office Surface Exchange Scheme).

2.2. Experimental design

Glacial simulations were run with Last Glacial Maximum boundary conditions following the PMIP4 protocol for 21 ka BP [78] using the GLAC-1D ice sheet reconstruction [79–82]. All simulations were initialized from *Romé22*'s Last Glacial Maximum control simulation, which has no meltwater. The Last Glacial Maximum control simulation was initiated from a previous set of HadCM3 Last Glacial Maximum simulations with PMIP3 conditions (i.e., 190 ppm atmospheric pCO_2, 21 ka BP orbital configuration, and a Last Glacial Maximum ice sheet [87]). It was then spun up for 3,500 years with the PMIP4 Last Glacial Maximum conditions, and then run for an additional 4,000 years for comparison to the other simulations run by *Romé22*. We began our simulations from year 1,000 of the additional 4,000 years.

Romé22 derived a transient meltwater history from GLAC-1D's reconstruction of the last deglaciation global ice sheet evolution, and then selected six different meltwater "snapshots" from fixed points in time along this transient meltwater history. The total salt content is also kept constant throughout the simulation by a salinity correction algorithm. We have selected their 20.7 ka BP snapshot simulation to further investigate. This simulation has consistent oscillations and a relatively uniform distribution of the 0.084 Sverdrup (Sv; 1 Sv is equal to 1 million cubic meters per second) meltwater forcing in the Arctic, GIN seas, and Western North America. In this study, we refer to *Romé22*'s *20.7k* simulation as *20.7k_Romé22*.

Our reference simulation, named *REF*, was performed with the same boundary conditions as *20.7k_Romé22* (see Table 1). We chose to rerun *20.7k_Romé22* to test the consistency of our results with those of *Romé22*. After noting that there was consistency in the results, we used *REF* as the primary simulation used to compare to the sensitivity tests.

We then performed six further simulations with the same meltwater forcing and paleogeography (including ice sheets) as *REF* to assess how sensitive our oscillations are to small and large changes in atmospheric CO_2 and orbital parameters (Table 1). Three simulations test changes in atmospheric CO_2 concentration—specifically a 10 ppm decrease (180 ppm), a 10 ppm increase (200 ppm), and a 20 ppm increase (210 ppm)—keeping the orbital configuration consistent with *REF*. These CO_2 concentrations represent high and low concentrations between 50 and 20 ka BP (atmospheric CO_2 concentration dipped to approximately 180 ppm around 25 ka BP, when ice sheets were at their largest extent; Figure 1d), and happen to fall roughly within the "window of opportunity" for climate oscillations identified by [68] in a different set of simulations performed with HadCM3, CCSM4 (Community Climate System Model 4), and MPI-ESM (Max Planck Institute Earth System Model). The other three simulations test the influence of changes in Earth's orbit, using triads of obliquity, precession, and eccentricity parameters corresponding to 30, 21.5, and 10 ka BP, but keeping atmospheric CO_2 concentration consistent with *REF*. Conditions at 30 ka BP are closest to MIS3, when D-O cycles were prevalent. We use 21.5 ka BP to investigate the impact of a small 500-year shift in time from the 21.0 ka orbit of *REF*. The 10 ka BP period was selected to explore how a high boreal seasonality and higher level of summer insolation at 65°N, the latitude of much Northern Hemisphere ice, would impact our oscillations. Thus, in each simulation, all initial and boundary conditions remained the same as in *REF* and *20.7k_Romé22* except for the condition tested (i.e., either atmospheric CO_2 concentration or orbital configuration year; Table 1).

Because HadCM3 relies on stochastic parameterization, we test the impact of stochastic variability on the oscillating simulations by repeating two simulations using exactly the same boundary conditions/forcings, but introducing some slight noise to the initial condition—the *REF* simulation and *Orbit_21.5k*. They are labeled *REF2* and *Orbit_21.5k2*, respectively (see Table 1). Thus, *REF*, *REF2*, and *20.7k_Romé22* are triplets

Table 1. Table of simulations showing the differences in boundary conditions and integration length. All other aspects of model configuration are identical across the experiments.

Simulation	Atmospheric CO_2 (ppm)	Orbital configuration year (ka BP)	Integration length (years)
20.7k_Romé22	190	21	10,000
REF	190	21	6,000
CO_2_180ppm	180	21	6,000
CO_2_200ppm	200	21	6,000
CO_2_210ppm	210	21	6,000
Orbit_10k	190	10	6,000
Orbit_21.5k	190	21.5	6,000
Orbit_30k	190	30	6,000
REF2	190	21	6,000
Orbit_21.5k2	190	21.5	6,000

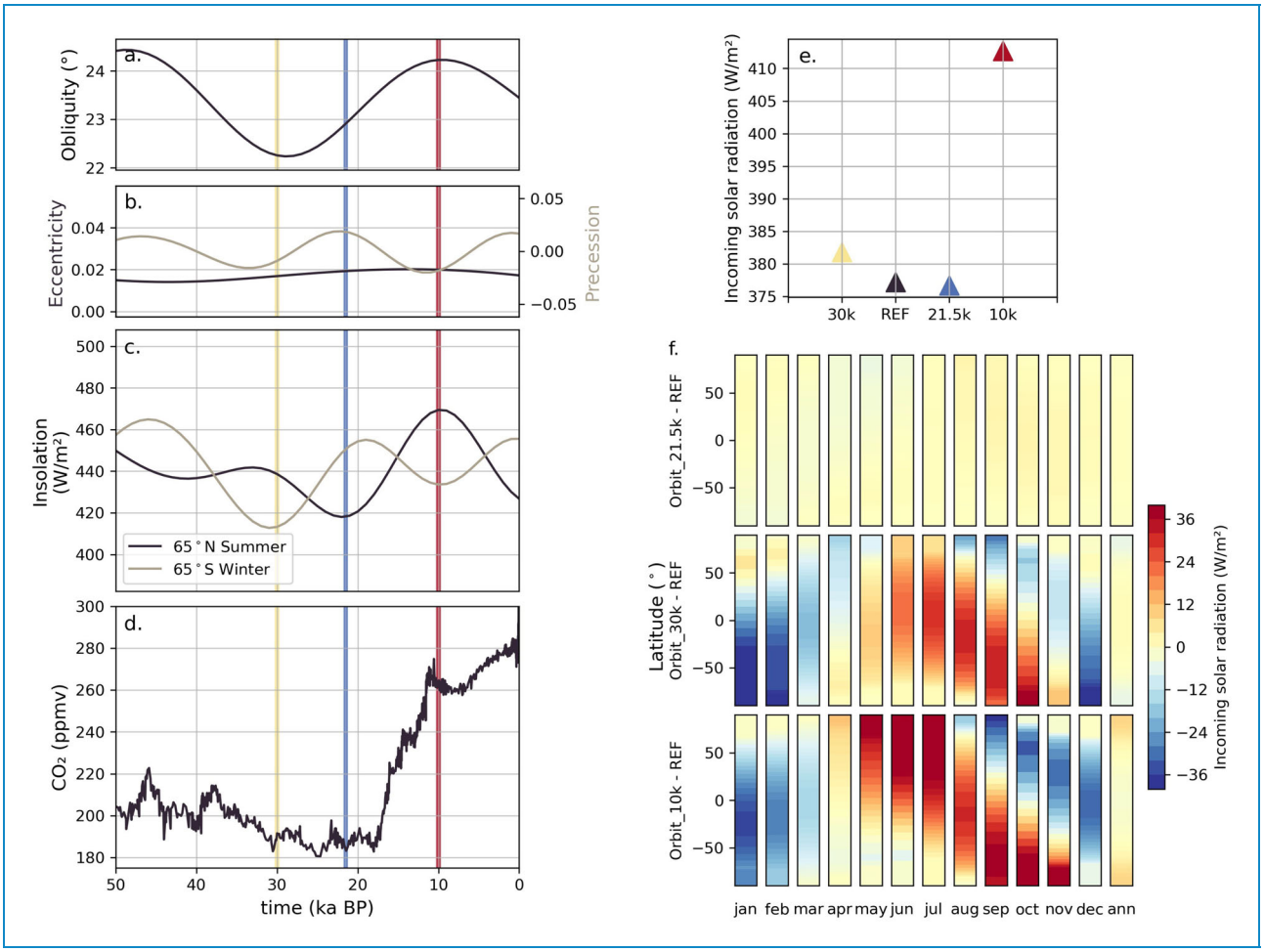

Figure 1. (a and b) Earth's orbital variation and (c) the impact on incoming solar radiation at the top of the atmosphere throughout the last 50,000 years [88]. The last 150,000 years are presented in the (Supplementary information Figure S1). (d) Atmospheric CO_2 concentration throughout the last 50,000 years [89]. (e) Quantification of boreal seasonality strength, calculated as the anomaly between median June–July–August incoming solar radiation and median December–January–February solar radiation, for the experiments testing orbital parameter changes and *REF*. (f) Incoming solar radiation anomalies from *REF* for each latitude in each month of the year.

and *Orbit_21.5k* and *Orbit_21.5k2* are twins. An analysis of their differences is described in Section 3.4.

2.3. Defining AMOC modes

For this analysis, we define the different states of the climate systems through several *modes* of North Atlantic deep convection (as described by *Romé22*). Because the AMOC regime does not change for a given deep-water formation pattern, we call them strong (or warm) and weak (or cold) corresponding to the strength of the AMOC (defined as the maximum of the Atlantic-basin meridional streamfunction at 26.5°N). We prefer the use of the cold and warm terminology to the stadial and interstadial terminology due to the use of a quasi-idealized experimental design that was not aimed to reproduce D-O conditions. The regions of interest in the modes' definition are given by the maps in Figures 4e and 5f.

We follow *Romé22*'s definition of five separate phases in our simulated oscillatory cycles corresponding to three modes of North Atlantic deep convection (*cold*, *meridional*, *zonal*) along with two transitionary phases (*warming*, *cooling*). The *cold* phase occurs when the system remains in a *cold* mode, characterized by the a weak convection over the entire North Atlantic (see fig. 7 of *Romé22* and our Figure 2a). Following *Romé22*, we define two separate warm modes, labeled after the geographic disposition of convection in the North Atlantic: the *meridional* mode, with the GIN seas as the dominant location for convection and weaker convection in the Irminger Sea (Figure 2b); and the *zonal* mode with convection primarily occurring in the Iceland/Irminger basins and weaker convection in the GIN seas (Figure 2c). The *warming* phase corresponds to the transition between the *cold* mode and any of the *warm* modes, and the *cooling* phase occurs between any of the *warm* modes and the *cold* mode. Note that the shorter *meridional* phase is sometimes

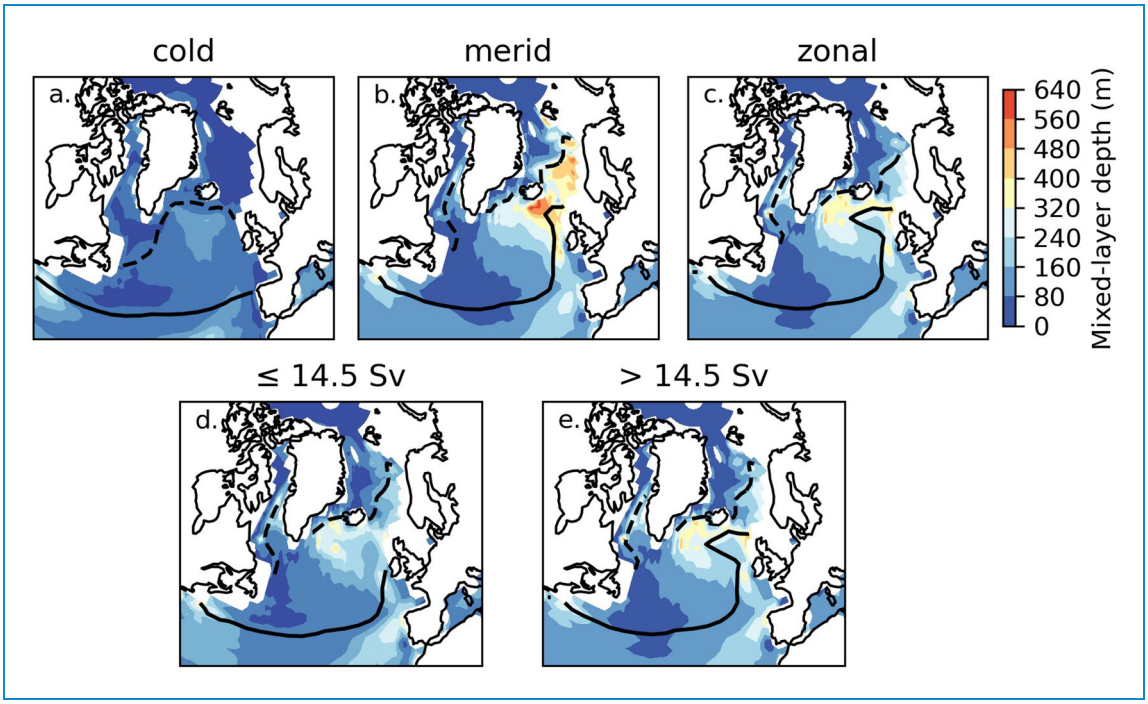

Figure 2. (a–c) December–January–February mixed-layer depth for *REF* averaged over each of the convection modes—*cold*, *meridional* (*merid*), and *zonal*. (d–e) As for (a–c), but with *Orbit_10k* representing the state of convection when the Atlantic Meridional Overturning Circulation (AMOC) is less than or equal to 14.5 Sv (d) and when the AMOC is greater than 14.5 Sv (e).

referred to as an AMOC overshoot mode as it always occurs after a *warming* phase. The system always travels across the oscillatory cycle in the same order: a cold AMOC, *cold* phase is followed by an AMOC recovery during the *warming* phase, succeeded by the *meridional* phase. Then a shift in North Atlantic deep convection moves the system into the *zonal* phase before a final AMOC weakening during the *cooling* phase brings the system back to the *cold* phase. This oscillatory cycle takes about 1,500 years (see *Romé22* for more detail).

When simulations are not oscillating, we will talk of *cold*, *meridional* and *zonal states* to describe the time spans when the system is set in a certain mode. Although they are different to the *phases* by definition, we will compare the *states* and *phases* indistinctively when they correspond to the same mode. For certain simulations, the three modes defined previously are not enough to describe all the AMOC states. We will therefore introduce more generic terminology of "dominant" and "moderate" AMOC modes. The *dominant* mode is attained when the convection pattern resembles the *zonal* mode and AMOC strength exceeds 14.5 Sv (Figure 2e). The *moderate* mode is attained when the convection pattern resembles a weaker *zonal* mode and the AMOC is less than or equal to 14.5 Sv (Figure 2d). We use the term *moderate* because the AMOC never drops below 10 Sv for CO_2_*200ppm*, CO_2_*210ppm*, and *Orbit_10k*, whereas in the *cold* mode the AMOC weakens to below 10 Sv.

To alleviate the challenges of comparing the *REF* simulation in a particular mode and the simulations in which the AMOC does not weaken below 10 Sv, in these instances, we define *REF* in the same format as in the simulation it is compared to. For instance, when comparing *Orbit_10k* in the *dominant* mode to *REF*, we compare to the instances of *REF* where the AMOC is greater than 14.5 Sv.

To create composite descriptions of the different modes in a simulation, the initial 1,000 years are excluded to remove the early spin-up period when the AMOC is adjusting to changes in climate forcing. Periodicity is measured as the average total time of each mode.

3. Results

Six new sensitivity experiments are presented here to understand the impact of CO_2 and orbital configuration on oscillatory-like behavior in our simulations (Figure 3). In all simulations, there is an initial spin-up period where the climate system adjusts to the updated climate forcings. This is evident in the sharp decrease in AMOC strength and Greenland surface air temperature, followed by an abrupt increase in ocean circulation strength of ~10–15 Sv in all simulations. All of the simulations are characterized by oscillatory behavior except for the higher CO_2 simulations (CO_2_*200pm* and CO_2_*210ppm*).

3.1. The reference simulation

The *REF* simulation is used as a benchmark for comparison between the new simulations presented here and

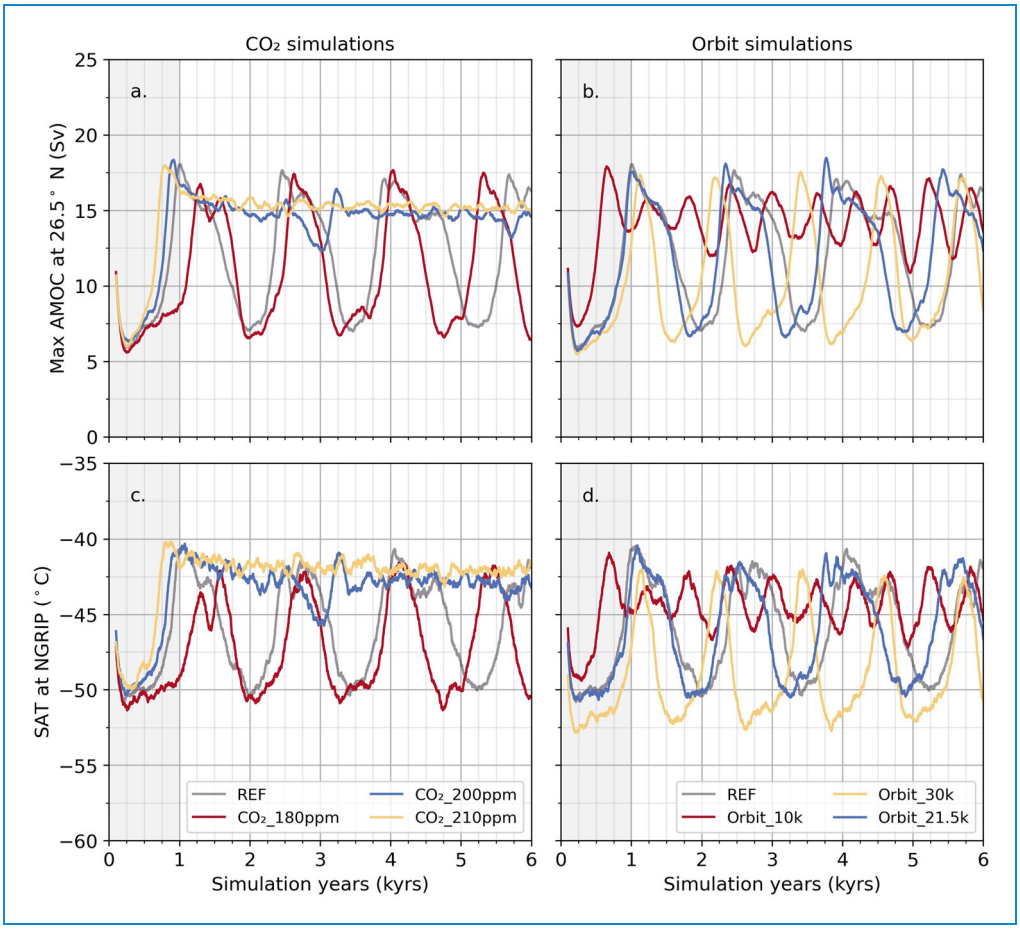

Figure 3. Top row: maximum Atlantic Meridional Overturning Circulation (AMOC) strength at 26.5°N for the simulations with changed CO_2 concentration (a) and for the simulations with changed orbital configuration (b). Bottom row: Surface air temperature (SAT) at NGRIP (North Greenland Ice Core Project; 42.32°W, 75.01°N) for the CO_2 (c) and orbit (d) simulations. Data are shown as 100-year rolling means. The 1,000-year spin-up period is shaded in gray.

the work of *Romé22*. In the *REF* experiment, oscillations have a periodicity close to 1,500 years with an AMOC strength spanning from ~6 to 17 Sv. As the climate system transitions into the oscillatory cycle, we can use a diagram of mixed-layer depth in the Irminger Sea as a function of mixed-layer depth in the GIN seas to identify the different phases of the cycle (Figure 4a). The *REF* simulation follows the same cycle than identified in *Romé22* (*cold–warming–meridional–zonal–cooling*) in roughly the same time (around 1,500 years).

3.1.1. The convection–advection mechanism

Romé et al. [83] introduced the convection–advection oscillator mechanism to explain the millennial-scale variability simulated in the HadCM3 *Romé22* set of simulations. This simulation relies on the coupling between the fast changes of stratification in the North Atlantic and the slow global reorganization of salt content through abrupt changes of the AMOC. By looking at the global salt transport between the Atlantic and the Pacific Ocean basins, we can first establish whether the simulations here follow the same mechanism as the simulations in *Romé22*.

Figure 5 shows the salt content budget of the six sensitivity experiments and *REF*. Whilst in the *cold* mode, salinity accumulates in the subtropical Atlantic. Eventually, this high concentration of salt leaks into the upper North Atlantic due to gyre circulation, reaching high-latitude regions like the GIN seas (see [83] for salinity tendencies). The leakage into the GIN seas causes the salinity and density of the surface ocean to increase. Stratification then decreases, allowing deep convection to restart, passing a threshold and re-invigorating the AMOC into the *meridional* mode. This threshold can be seen in the density anomaly in the GIN seas between 500 and 50 m (Figure 6b). Whilst convection is strong, salinity is transported around the globe to ocean basins that lost salt to the subtropics during the *cold* mode (e.g., the Pacific Ocean; Figure 5). As the subtropical Atlantic becomes depleted in salt, salinity in the GIN seas begins to decrease alongside surface density, causing stratification to increase again until a threshold is crossed, whereby the AMOC weakens abruptly. This circulation of salinity throughout the

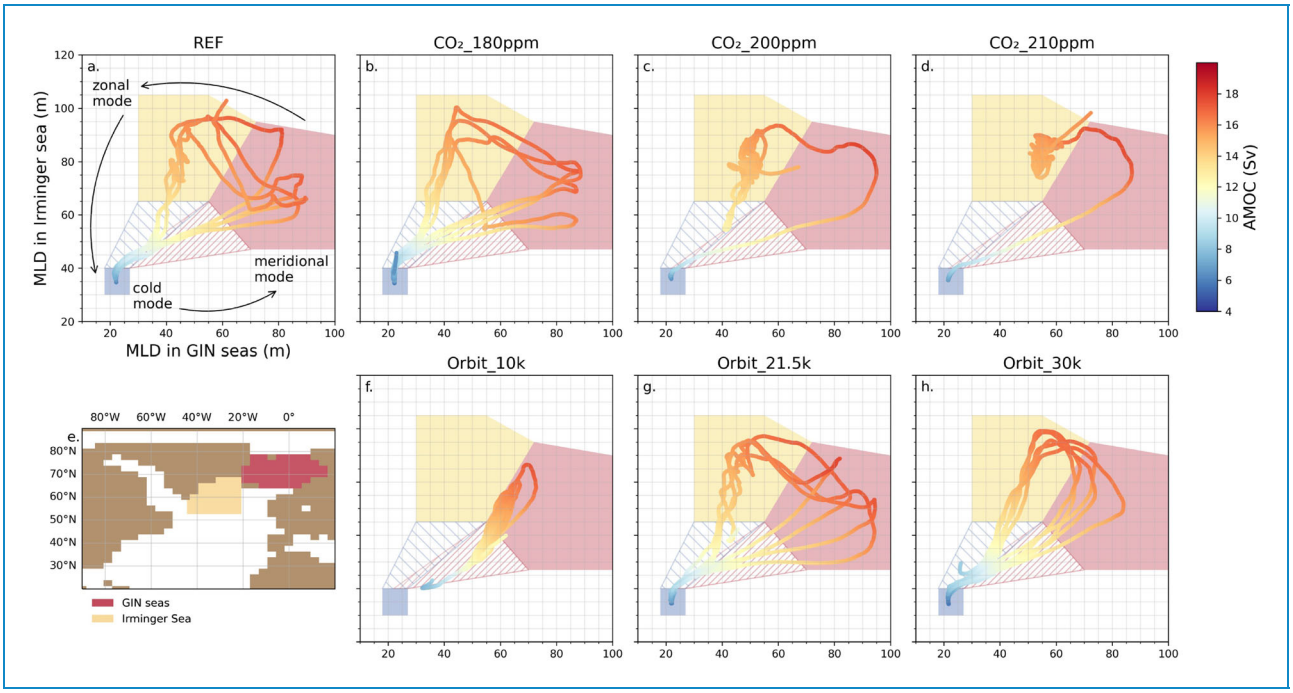

Figure 4. (a–d) and (f–h) Mixed-layer depth (MLD) in the Irminger Sea as a function of mixed-layer depth in the Greenland, Iceland, and Norwegian (GIN) seas with the colors representing maximum strength of the Atlantic Meridional Overturning Circulation (AMOC) at 26.5°N. Red shading represents the *meridional* phase, yellow shading is the *zonal* phase, and blue shading represents the *cold* phase. The red hatched region is the transition between the *cold* and *meridional* phase (or the *warming* phase), and the blue hatched region is the transition between the *zonal* and *cold* phase (or the *cooling* phase). (e) The map of the North Atlantic illustrates which locations are used to represent the GIN seas and the Irminger sea. The color of the location corresponds to the color of the mode in which convection is strongest in the region.

ocean basins is a key control in the change of stratification in the sea basins and vice versa, oscillating with the same periodicity as the AMOC (Figure 6a,b). We also observe salinity changes in the Southern Ocean due to the strengthening and weakening of the Antarctic bottom water during the warm and cold regimes (Supplementary Figure S2). However, these changes are too weak to drive significant changes in Antarctica Bottom Waters formation that could influence the mechanism [83]. In other simulations with higher sensitivity to Antarctic bottom water, these salinity changes could be more effective [90].

The transport of salt from the subtropical Atlantic to the North Atlantic and Pacific is evident in the spin-up period of each simulation and continues in the experiments that oscillate fully from cold to warm regimes (gray region in Figure 3). However, this mechanism alone cannot explain the changes in the periodicity of simulated AMOC oscillations relative to *REF*. For instance, changes in the CO_2 level or orbital configuration are shown to impact the oscillatory pattern shown in *REF* by increasing the speed of the oscillations, disrupting the shape and amplitude, or ceasing oscillations all together (Figure 3). A faster mechanism is also required to explain the centennial-scale, as opposed to millennial-scale, oscillations present in *Orbit_10k* (Section 3.3). We hypothesize that sea ice impacts the pace of the convection–advection mechanism, as the sea ice volume and transport controls the salinity content in the GIN and Irminger seas. The changes in CO_2 concentration and boreal seasonality provide new insight into the role of sea ice, including the part it plays in controlling the speed at which the AMOC can switch between warm and cold regimes.

3.2. Impact of CO_2 on the oscillatory regime

Three sensitivity experiments were run to test the effect of CO_2 concentrations (180, 200, and 210 ppm). The higher CO_2 concentration simulations reach a *dominant* AMOC steady state after the initial spin-up period and remain in the *dominant* state for the rest of the simulation besides for two small excursions into a *moderate* state in the 200 ppm simulation (Figure 3a). The lower *CO2_180ppm* simulation, on the other hand, oscillates at a quicker pace than *REF*, with an overall weaker AMOC that remains in a warm phase for a shorter period of time. From these simulations, we determine that CO_2 concentration controls the strength of the AMOC, whether oscillations can occur, and the duration of the warm and cold phases.

3.2.1. Low atmospheric CO_2 concentration

The *CO2_180ppm* simulation represents the lowest end of atmospheric CO_2 concentration during the last 50,000 years (Figure 1d). This lower CO_2 simulation oscillates with a periodicity ~200 years shorter than *REF*

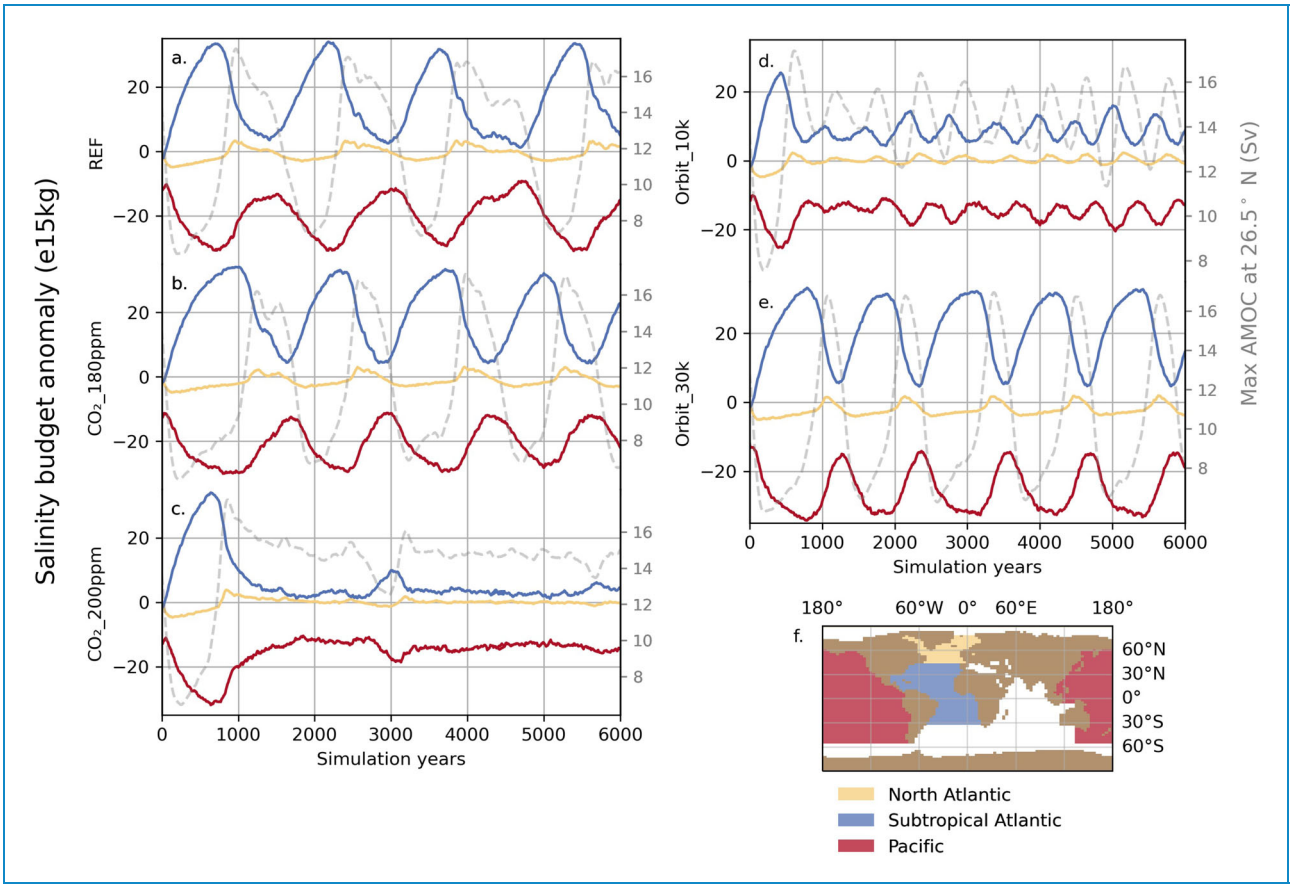

Figure 5. (a–e) Salinity budget anomaly from Last Glacial Maximum conditions in three ocean basins: North Atlantic, Subtropical Atlantic, and Pacific Ocean. Maximum AMOC strength at 26.5°N is also shown (gray dashed line) to easily identify when the simulation is in a warm or cold regime. (f) Map illustrating how the extent of each region is defined. *CO_2_210ppm* and *Orbit_21.5k* are similar to *CO_2_200ppm* and *REF*, respectively, and so are left out of this figure for simplicity. Last Glacial Maximum conditions are defined by *Romé22's CTRL_LGM* simulation with an AMOC strength at ∼15 Sv.

(Figure 3). The cycling between the *cold*, *zonal*, and *meridional* phases still occurs in this simulation, as it does in *REF* (Figure 4b), but the transitions between the *meridional* and *zonal* phases are more abrupt and less consistent between cycles. The length of the warm phases decreases (by ∼300 years, on average) and although the length of the *cold* phase increases (by ∼100 years, on average), overall, the periodicity of the simulation is shorter. This suggests that the lower CO_2 concentration favors the warm phases of the oscillation to the detriment of the cold phase, in accord with the results of [58] and [91].

Lower surface temperatures in the *CO_2_180ppm* simulation (Figure 7a–c) lead to increased Northern Hemisphere sea ice volume in every AMOC phase compared to *REF* (∼43×10^5 km^3 on average in the warm phases; Figure 8). When CO_2 concentration is lower, the sea surface remains colder relative to the warmer and higher CO_2 climates (Figure 7a–c), allowing sea ice to return more quickly from the warm modes (Figure 9b,c). In addition, the colder surface temperatures promote thicker sea ice in the Arctic and northern North Atlantic (Supplementary Figure S3), resulting in warmer subsurface temperatures under the sea ice (Supplementary Figure S4a). As the AMOC strengthens, enhanced convection in the GIN and Irminger seas pushes sea ice southward and proximal sea ice melts. However, because the sea ice volume is larger, it contributes ∼4.2% more fresh water than *REF* (faster decrease of sea surface salinity in Figure 6d) and more sea ice transport (Figure 9d) to sites of deep water formation during the warm modes. The rapid decrease in salinity concentration from the melting sea ice paired with the warmer subsurface temperatures decreases upper North Atlantic density and increases stratification of the water column, hindering the AMOC's ability to sustain its strength in the *zonal* phase and moving the climate out into the *cold* phase again (following Paths (a) and (b) in Figure 10). Thus, greater sea ice volume and transport are linked to a shortened warm mode compared to *REF*.

3.2.2. High atmospheric CO_2 concentration

In contrast to *CO_2_180ppm* and *REF*, the *CO_2_200ppm* simulation does not oscillate. During the spin-up period (the first 1,000 years of simulation), the AMOC in *CO_2_200ppm* travels through the initial stages of the *cold–meridional–zonal* cycle, first dropping into the *cold*

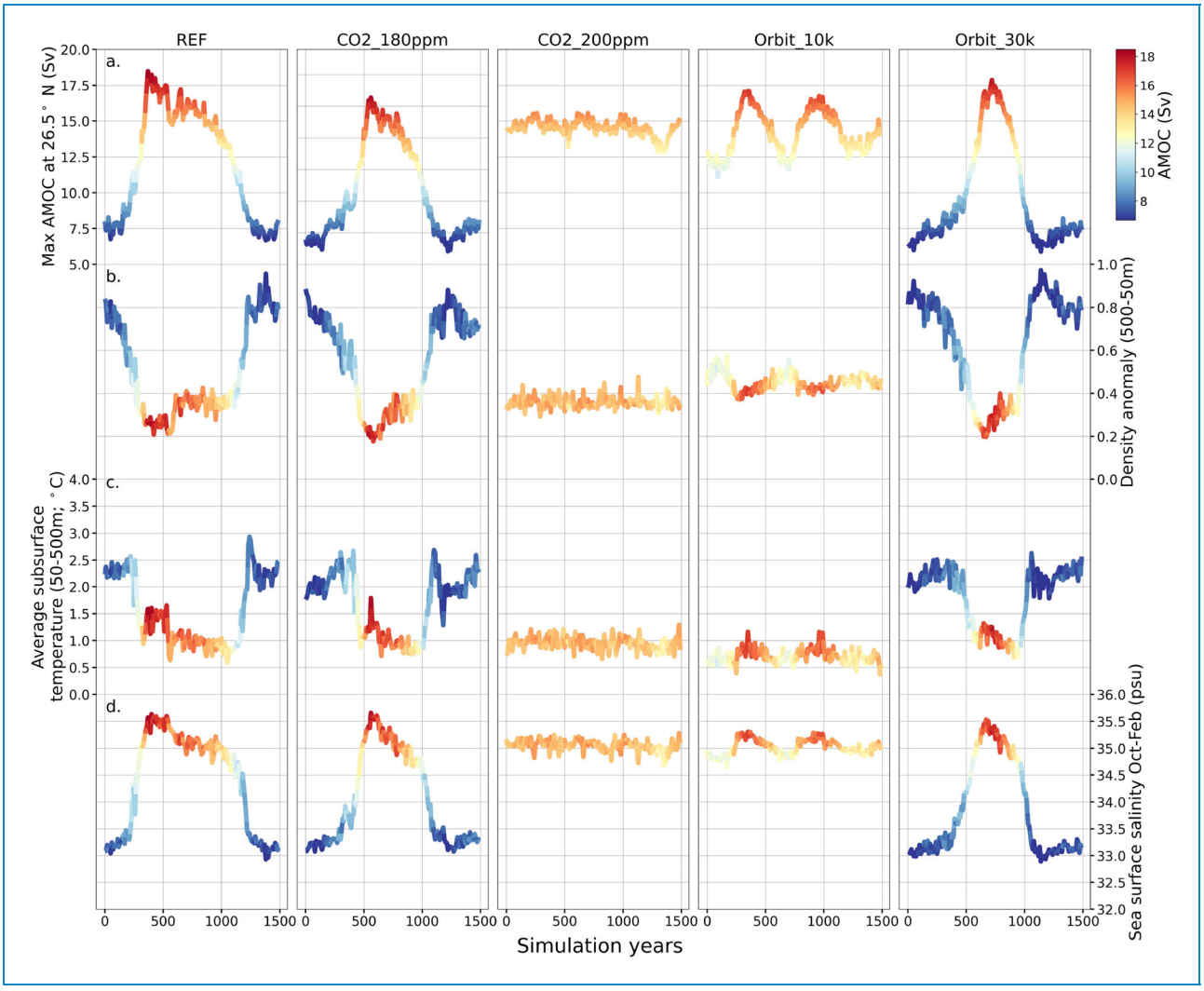

Figure 6. (a) Maximum Atlantic Meridional Overturning Circulation (AMOC) strength at 26.5°N; (b) density anomaly between 500 and 50 m for the Greenland, Iceland, and Norwegian (GIN) seas; (c) mean ocean temperature between 50 and 500 m depth in the GIN seas; (d) sea surface salinity in the sea ice formation months (October to February) in the GIN seas for the length of one oscillation of the *REF* simulation. The color map is normalized to the max AMOC strength in *REF* (a) as shown in the color bar. All data are shown as decadal means. *CO_2_210ppm* and *Orbit_21.5k* resemble *CO_2_200ppm* and *REF*, respectively, and so are left out of this figure for simplicity.

phase, then rapidly transitioning through the warm *meridional* phase and on to the *zonal* phase (Figure 4c). Thereafter, *CO_2_200ppm* mainly remains in a *zonal* state, with an AMOC strength of ~15 Sv. Nonetheless, the *CO_2_200ppm* simulation does show signs of instability. Around ~2,500 years into the run, AMOC weakens by ~2.5 Sv, instigating a transition to the *cold* state (Figure 4c), but AMOC quickly recovers to the *zonal* state after ~700 years. This sequence occurs again on a smaller scale ~5,750 years into the run. During the first period of instability and reduced AMOC strength, the surface air temperature in the North Atlantic and Greenland decreases by ~4 °C. This temporary excursion is reminiscent of the 8.2 kyr event (an abrupt cooling of 1–3 °C that lasted ~160 years in the Northern Hemisphere [92,93]), raising the question of whether some century-long AMOC perturbations could be intrinsic rather than forced by a meltwater pulse.

Adding an additional 10 ppm of CO_2 to the atmosphere appears to safely stabilize the AMOC in a warm state for the entirety of the *CO_2_210ppm* simulation, after the spin-up period. The AMOC remains at ~15 Sv from year 1,500 to the end of the simulation, surface air temperature stays warmer than *REF* at most locations (Figure 7l,m), and there is the least Northern Hemisphere sea ice volume in the *dominant* state compared to the other CO_2 sensitivity simulations and *REF* (Figure 8).

The warmer surface temperatures in both simulations lead to thinner and sparser sea ice (Figures 8 and 9b,c) compared to *REF*. The atmosphere–ocean heat exchange increases, causing North Atlantic

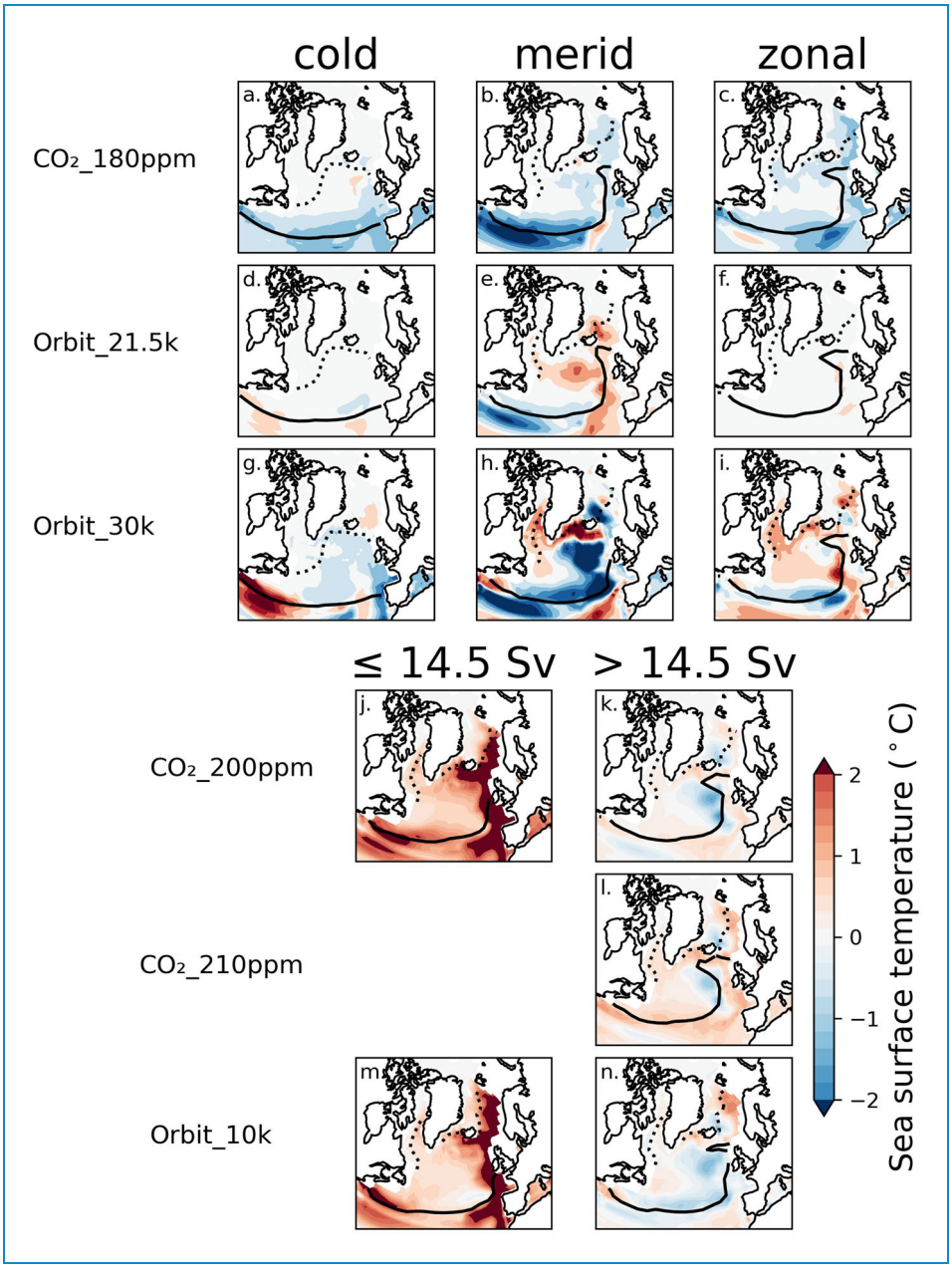

Figure 7. (a–i) Annual sea surface temperature anomaly from *REF* averaged for each Atlantic Meridional Overturning Circulation (AMOC) mode (*cold*, *meridional*, and *zonal*). (j–n) Same as (a–i) but AMOC modes are defined by "*dominant*" (greater than 14.5 Sv) and "*moderate*" (10–14.5 Sv) for *CO_2_200ppm*, *CO_2_210ppm*, and *Orbit_10k* and *REF* is defined by "*dominant*" (greater than 14.5 Sv) and "*moderate*" (less than or equal to 14.5 Sv). There is no *moderate* mode for *CO_2_210ppm*. For all, the solid line depicts March sea ice extent (15% cover) and the dashed line depicts September sea ice extent.

temperatures to decrease at depth (Supplementary Figure S4j–m). Stratification in the North Atlantic, therefore, is lower, and simultaneously, salinity concentration is consistently higher (Figure 6b,c) due to minimal sea ice transport (Figure 9d). Because of these factors, it is more difficult to pass the stratification threshold that forces AMOC to weaken.

The shift from a *cold–meridional–zonal* cycle to a *dominant–moderate* variability pattern is not only obtained by changing the background CO_2 concentration to 200 ppm, but also occurs when the orbital configuration is modified as in *Orbit_10k*. We describe these changes of behaviors in the next section.

3.3. Impact of orbital configuration on the oscillatory regime

We performed three sensitivity experiments to test the impact of orbital configurations throughout the last 50,000 years (*Orbit_30k*, *Orbit_21.5k*, and *Orbit_10k*). In these simulations, the year of the orbital configuration

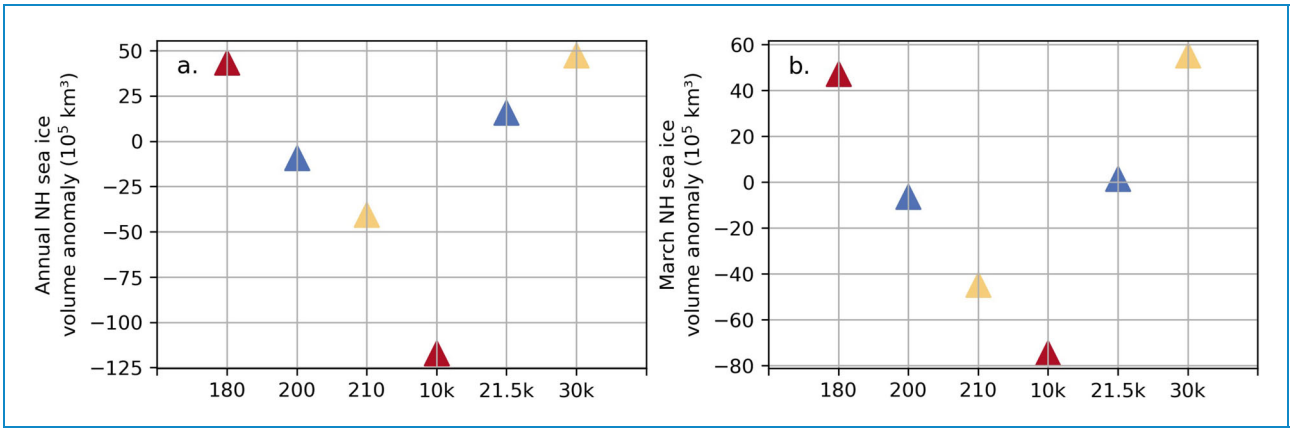

Figure 8. (a) Annual mean Northern Hemisphere (NH) sea ice volume anomaly from *REF* for each simulation. (b) As for (a), but in March. For both panels, the anomaly is calculated as an average for the warm modes (inclusive of the *zonal* and *meridional* phases) for the simulations that exhibit full oscillations (CO_2_*180ppm*, *Orbit_10k*, and *Orbit_21.5k*). In contrast, for *Orbit_10k*, CO_2_*200ppm*, and CO_2_*210ppm*, the anomaly is calculated as an average of when the AMOC is greater than 14.5 Sv for *REF* and the named simulations.

is changed from *REF*, and therefore includes differences in the obliquity, eccentricity, and precession of the Earth (Figure 1a,b). From these simulations, we determine that insolation changes due to the different obliquity lead to localized climate effects that have the strongest impact on the AMOC regimes and, in turn, the oscillating patterns (Figure 1f).

3.3.1. Low boreal seasonality (Orbit_21.5k)

Insolation at 21.5 ka BP is most similar to the *REF* experiment. Boreal summer insolation in the Northern Hemisphere at 21.5 ka BP is only ∼0.31 W m^{-2} less than the 21 ka BP orbit. Precession is slightly closer to 90°, and obliquity has decreased (Figure 1a,b). This orbital configuration results in a weak boreal seasonality, also slightly weaker than in *REF* (Figure 1e). Oscillations in the *Orbit_21.5k* simulation have a similar amplitude to *REF* (Figures 3 and 4g). Surface temperatures are very comparable to *REF* especially in the *cold* and *zonal* modes (Figure 7d–f). In the *meridional* mode, the North Atlantic in *Orbit_21.5k* is ∼1 °C warmer, potentially linked to the increased annual sea ice volume (Figure 8a).

3.3.2. Strong boreal seasonality (Orbit_30k and Orbit_10k)

The *Orbit_30k* simulation emulates the effect of an orbital configuration from the end of Marine Isotope Stage 3, a period when cycles between weak and strong AMOC (D-O cycles) were common, on simulated millennial-scale variability. The insolation is 20 W m^{-2} higher than at 21 ka BP, but obliquity has decreased from a median degree to a low point (from 23 to 22°). Precession is at ∼220° and eccentricity has decreased a small amount from *REF* (Figure 1a–c). As precession nears 270°, the boreal seasonality increases in strength. As shown in Figure 1e,f, *Orbit_30k* has the second strongest boreal seasonality of the ensemble, after the *Orbit_10k* simulation.

The oscillations in *Orbit_30k* have a shorter periodicity and faster transition time from *warm* to *cold* modes compared to *REF* (Figure 3). The AMOC briefly passes through the *meridional* and *zonal* phases (in a warm phase for ∼300 years on average compared to ∼700 years for *REF*) before transitioning back into the *cold* mode (Figure 4h) which lasts on average ∼60 years longer than in *REF*. Despite the increase in Northern Hemisphere insolation, North Atlantic sea surface temperatures (Figure 7g–i) in the *cold* and *meridional* phases and surface air temperature at the North Greenland Ice Core Project (NGRIP) location in Greenland (Figure 3) are ∼1–2 °C colder than *REF* (Figure 7g–i).

In the *Orbit_10k* simulation, summer Northern Hemisphere insolation further increases to ∼469.5 W m^{-2}, another 30 W m^{-2} greater than the *Orbit_30k* simulation. Obliquity is close to the highest value (∼24°), and precession is very close to 270°. *Orbit_30k* and *Orbit_10k* have obliquity values at opposite ends of the spectrum. Because of this, the pattern of incoming solar radiation is different, impacting the seasonality distribution. For instance, *Orbit_10k* has stronger incoming solar radiation in the Northern Hemisphere in the boreal summer months, as well as in the Southern Hemisphere during the boreal winter months (Supplementary Figure S5). *Orbit_10k* has the weakest incoming solar radiation compared to *Orbit_30k* in the mid- to high Northern latitudes during the boreal winter months.

The periodicity of the oscillations in *Orbit_10k* is significantly shorter than *REF* (∼500 years). After the initial spin-up, AMOC strength rapidly oscillates between ∼12 (*moderate* phase) and 18 Sv (*dominant* phase) and Greenland temperature transitions between ∼ −37 and −43 °C, respectively, but note that each oscillatory cycle varies in amplitude (Figure 3). During these quick oscillations, the AMOC never reaches the *meridional* phase,

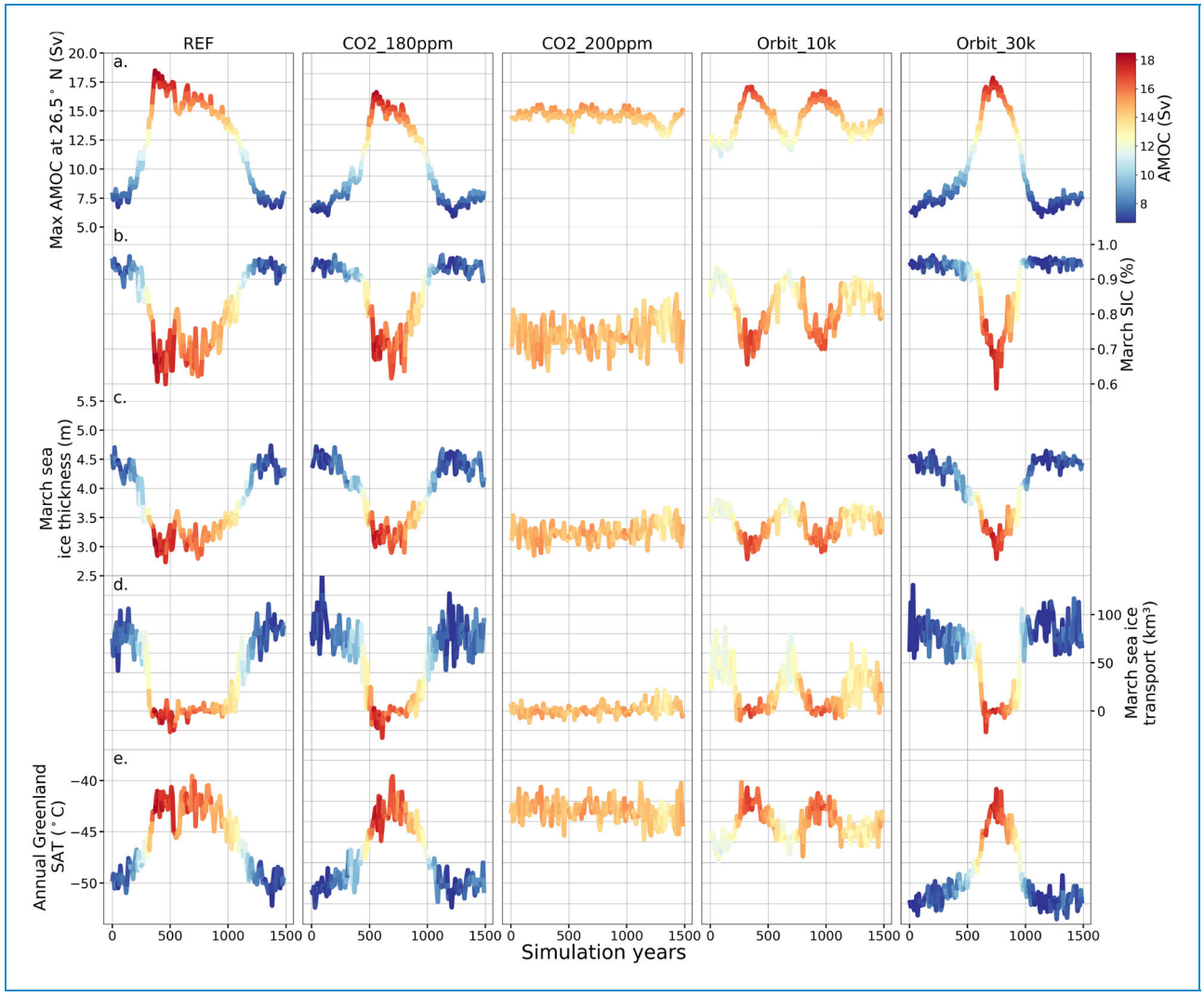

Figure 9. (a) Maximum Atlantic Meridional Overturning Circulation (AMOC) strength at 26.5°N; (b) March sea ice concentration (SIC) calculated between 50°N and 70°N; (c) sea ice thickness in March between 50°N and 70°N; (d) March sea ice transport defined as a zonal sum between 40°W and 0° at 60°N; and (e) annual surface air temperature (SAT) at the Greenland Summit for the length of one oscillation of the *REF* simulation. The color map is normalized to the max AMOC strength in *REF* (a) as shown in the color bar. All data are shown as decadal means. *CO_2_210ppm* and *Orbit_21.5k* are similar to *CO_2_200ppm* and *REF*, respectively, and so are left out of this figure for simplicity.

and neither does it return to the initial *cold* phase (Figure 4f). The ocean basins also have a smaller amplitude of salt content change (Figure 5d).

The speed at which the oscillations occur, centennial-scale instead of millennial-scale, implies that they do not follow the convection–advection mechanism, as more time is necessary to recirculate the salt between ocean basins. Instead, we hypothesize that the AMOC in *Orbit_10k* follows a pathway similar to the high CO_2 simulations. The strong boreal seasonality at 10 ka BP causes substantial increase in sea ice area each winter as well as substantial melt each summer. This is evident in the large seasonal sea ice variability in the GIN and Irminger seas (e.g., sea ice concentration increases from 25% in boreal autumn to 95% concentration in spring in the GIN seas during the *moderate* phase; Supplementary Figure S6). However, it also results in thinner sea ice throughout the year (Figure 9). As with *CO_2_200ppm* and *CO_2_210ppm*, the thinner sea ice results in an increased atmosphere–ocean heat flux and colder subsurface temperatures in the North Atlantic, leading to consistently low stratification and a warm AMOC (following Path (c); Figure 10).

Unlike *CO_2_200ppm* and *CO_2_210ppm*, in *Orbit_10k* sea ice extent reaches nearly the same maximum and minimum aerial cover as for *REF*, despite not reaching the same maximum and minimum high-latitude surface air temperatures or AMOC strengths (Figure 9). We hypothesize that the high sea ice concentration variability paired with the thin sea ice is the cause of the centennial-scale oscillations not present in the high CO_2 simulations. This is evident from the increased transport of sea ice in the GIN and Irminger seas during the *moderate* phase (Figure 9d), leading to fresher conditions in the convection sites and a weaker AMOC. When transport decreases and new sea ice forms (sea

ice concentration increasing; Figure 9), the AMOC is able to recover into the *dominant* phase. We suggest that in the case of *Orbit_10k*, the sea ice variability is due to the strong boreal seasonality, but this requires further investigation beyond the scope of this study. The small excursions in *CO_2_200ppm* are also related to this process. Sea ice concentration is low and transport is nearly 0 km^3/yr throughout the simulation, except at the two small dips into the *moderate* phase when sea ice concentration and transport increases (Figure 9 and Supplementary Figure S7; but monthly ocean velocity was not available for *CO_2_200ppm* during the first and largest excursion into the *moderate* phase, so we could not calculate sea ice transport to robustly confirm that the same mechanism is followed as with the *Orbit_10k* oscillations).

On the other hand, *Orbit_30k* moves through the full oscillatory cycle similar to *REF*, just ~350 years faster. On average, the time spent in the *cold* phases is actually longer (by ~60 years) than for *REF*, but this is more than compensated for by the shortening (by ~400 years) of the time spent in a warm AMOC regime, very similar to *CO_2_180ppm*. The colder sea surface temperatures compared to *REF* (Figure 7g–i), due to the decrease in annual incoming solar radiation in the high latitudes compared to *REF* (Figure 1f), as well as the low obliquity at 30 ka BP (consistent with previous studies; e.g., [94]), sea ice volume accumulates in the Arctic and northern North Atlantic, and becomes even thicker than in *CO_2_180ppm* and *Orbit_10k* (Figure 8 and Supplementary Figure S5). This contributes an even larger amount of freshwater ($\sim 47 \times 10^5$ km^3 during the warm phases) and sea ice transport to sites of deep water formation when sea ice melts during the warm phases (Figures 8 and 9d) and subsequently, sea surface salinity decreases faster for *Orbit_30k* than *CO_2_180ppm*, producing a more rapid shift from the *zonal* to *cold* phase.

3.4. Variation between simulations of the same boundary conditions

Although the evolution of the oscillating simulations is mostly deterministic, stochasticity influences the precise shape and duration of the oscillations in our multi-millennial simulation ensembles. Small differences can be seen in the amplitude of AMOC changes, the duration of each phase, and the strength of deepwater formation. In our repeated subsection of simulations using exactly the same boundary conditions/forcings, we observe even larger discrepancies between the sets of triplets (i.e., *REF*, *REF2*, and *20.7k_Romé22*) and twins (*Orbit_21.5k* and *Orbit_21.5k2*).

The most remarkable difference between these simulations is that *REF2* and *Orbit_21.5k2* skip an oscillation compared to *REF* and *Orbit_21.5k*. In *REF2*, the second oscillation does not contain a *cold* phase (Figure 11). Similarly, in *Orbit_21.5k2* the first oscillation does not contain a *cold* phase (Supplementary Figure S8). Romé et al. [83] argue that *20.7k_Romé22* is close to reaching equilibrium in the salt budget at the end of the *zonal* phase, suggesting that this could, in rare cases, prevent

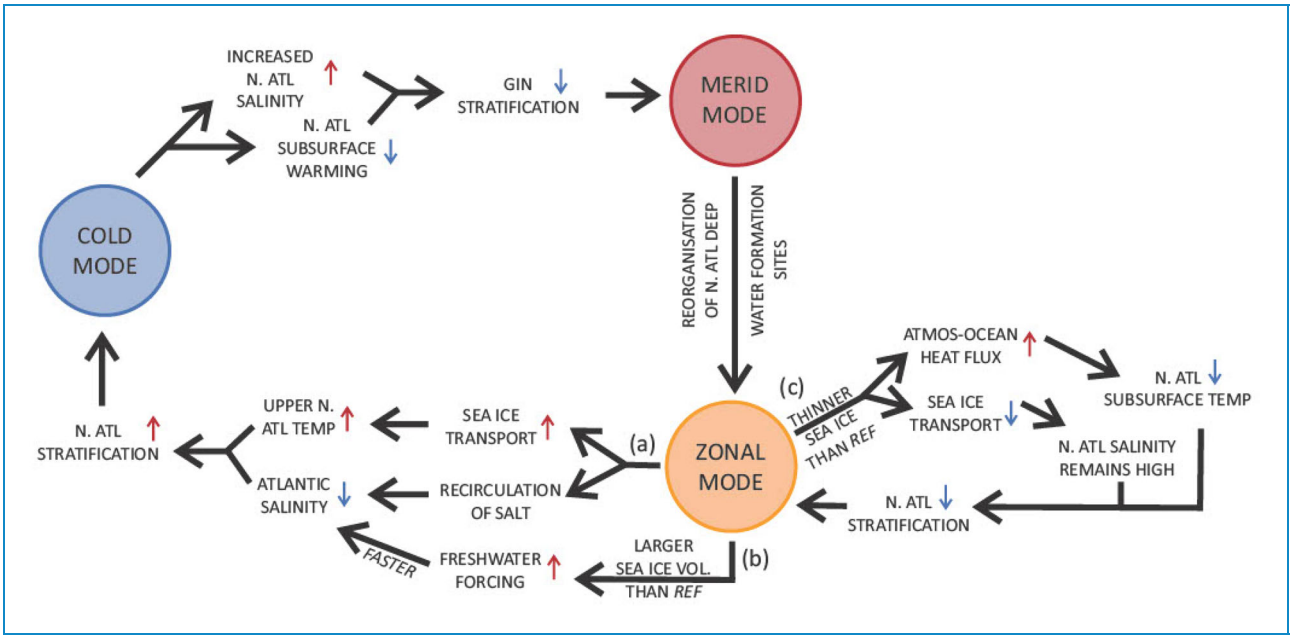

Figure 10. Update to the convection–advection mechanism. Path (a) represents the original convection–advection mechanism by Romé et al. [83], whereas paths (b) and (c) are new to this study: possible pathway (b) whereby larger sea ice volume leads to a faster transition between warm and cold Atlantic Meridional Overturning Circulation (AMOC) phases due to an increase in freshwater input; possible pathway (c) whereby less sea ice leads to an increase in the atmosphere–ocean heat flux and a decrease in temperature throughout the water column in the North Atlantic (N. Atl), allowing the AMOC to remain strong.

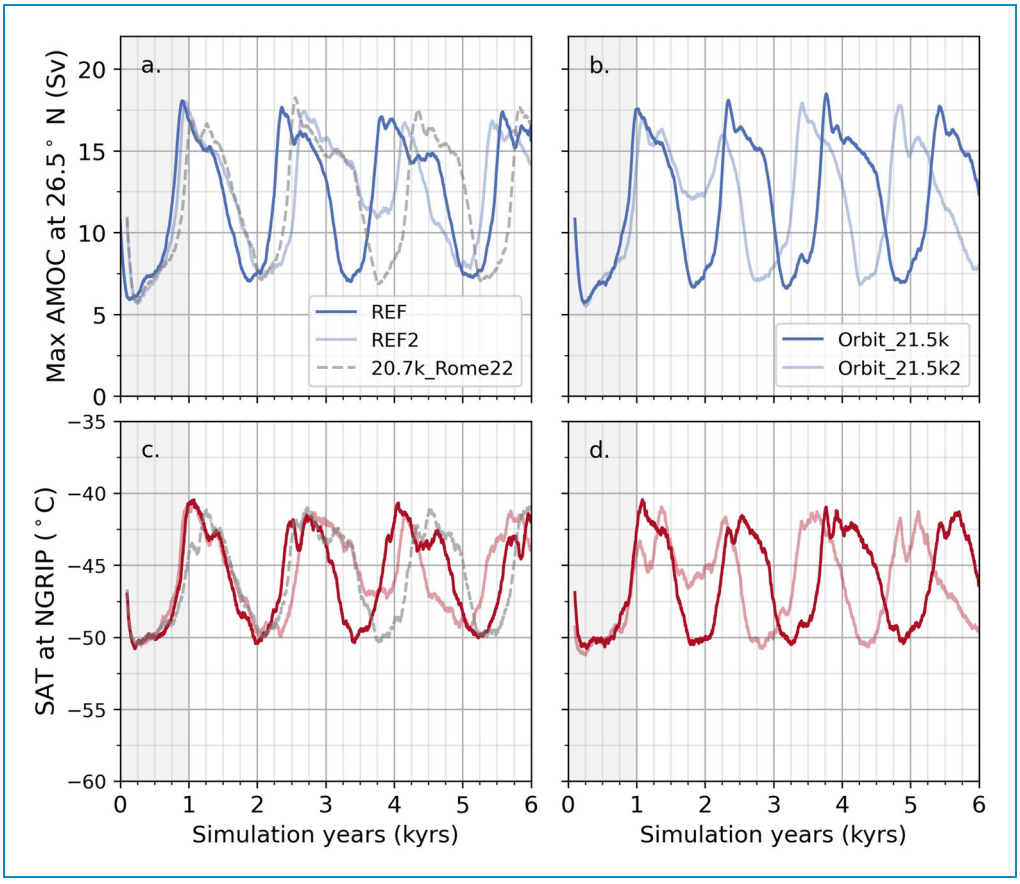

Figure 11. Top row: Maximum Atlantic Meridional Overturning Circulation (AMOC) strength at 26.5°. Bottom row: Surface air temperature (SAT) at NGRIP (North Greenland Ice Core Project; 42.32°W, 75.01°N). The original *REF* and *Orbit_21.5k* simulations are shown in the bolder colors, and the corresponding repeat simulations are shown in the paler colors. Data are shown as 100-year rolling means. The 1,000-year spin-up period is shaded in gray.

the system from entering a positive feedback leading to the abrupt deactivation of the North Atlantic deep water formation. Instead, the AMOC stalls in an extended warm phase, switching from a *meridional* phase to a *zonal* phase, before a slight weakening comparable to *CO_2_200ppm* and a recovery into a *meridional* phase. At the end of the *meridional* phase, the positive feedback is activated and the system switches to a *cold* phase. The skipping of the cold transition results in a 500-year offset between the *Orbit_21.5k* and *Orbit_21.5k2* cycles. There is less of an offset between the *REF* and *REF2* cycles by the end of the simulations due to the longer warm regime in the second oscillation followed by an oscillation with a warm regime 700 years shorter.

We propose that the differences in the evolution of the twin and triplet experiments are caused by the competing influences on ocean density of sea ice volume (which decreases North Atlantic salinity; Figure 10b) and thickness (which decreases subsurface temperatures; Figure 10c) and the standard convection–advection process of the depletion of salinity through ocean transport (Figure 10a). Because *20.7k_Romé22* and its siblings (*REF* and *REF2*) are operating in a very narrow "window of opportunity," variability in the sea ice thickness can determine whether the AMOC completes a full oscillatory cycle or returns to the *zonal* mode. In this case, less sea ice transport occurs compared to a full *cold–meridional–zonal–cold* cycle (Supplementary Figure S9g) and the oscillating pattern temporarily shifts to a shorter oscillation similar to *Orbit_10k*. During these oscillations, there is minimal change in the stratification in the GIN seas compared to a full cycle, but sea ice concentration still reaches a similar minimum and maximum as in the other cycles and sea surface salinity remains high (Supplementary Figure S8). Because sea ice is a stochastic and highly sensitive system, its feedbacks do not always dominate the climate trajectory, hence the stratification threshold from salinity reorganization and freshening from sea ice migration (as in the convection–advection mechanism [83]) is sometimes crossed first, allowing the AMOC to return to the *cold* phase, whereas in other cases, sea ice is thinner, allowing the convection sites to stay saline enough to reach the opposing stratification threshold and forcing the AMOC to return to the *zonal* phase.

In this section, we showed that stochastic variability can be responsible for modification in the duration of

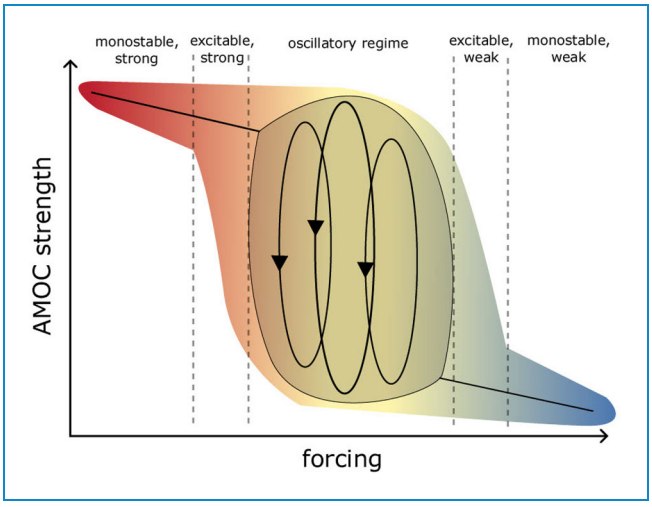

Figure 12. Bistability curve of Atlantic Meridional Overturning Circulation (AMOC) stability modes according to strength of forcing (e.g., ice meltwater flux or atmospheric pCO_2); a schematic view. The stability modes, separated by a dashed gray line, are labeled as such: a monostable and strong AMOC (e.g., *CO_2_210ppm*); an excitable, strong AMOC that occasionally gets pulled into a weaker mode (e.g., *CO_2_200ppm*); an oscillating AMOC (e.g., *REF*, *CO_2_180ppm*, and the orbit simulations); an excitable, weak AMOC that occasionally gets pulled into a stronger mode (e.g., *Romé22*'s *18.2k* simulation); and a monostable and weak AMOC (e.g., *P185* and *P149* from Klockmann et al. [53]). The gradient shape around the curve represents the range of possible AMOC variability within each mode.

one individual oscillating cycle. It cannot, however, modify the periodicity of several cycles by an order of magnitude, nor can it change the long-term mode of variability of a simulation.

4. Discussion

4.1. Controls on AMOC stability

Developing a robust understanding of earth system changes induced by climate forcings in complex models is difficult due to the wide variety of initial climate conditions and the potential non-linearity of responses across different models and different model experiments. Although multiple abrupt climate change events are positively correlated with transitions in the AMOC, how the AMOC is impacted by external forcings and the resultant response of the climate is still largely unknown. In this section, we have tried to capture and identify the impact of glacial-period changes in orbit and CO_2 on the ability of the AMOC to remain in or transfer between different modes of stability.

Previous studies [64,95,96] have visualized the stability of the AMOC with respect to external forcing, such as freshwater forcing, in the form of a bifurcation diagram. From our simulations and those of *Romé22*, we can offer a similar view inspired by classical bifurcation diagrams (Figure 12). For example, examining *Romé22*'s simulations with different meltwater forcings, we determine that as meltwater increases, the AMOC moves from a monostable, strong AMOC regime (e.g., *Romé22*'s *21.5k* simulation) to an oscillating regime (e.g., *Romé22*'s *20.7k* and *19.4k* simulations) to an excitable weak AMOC regime (e.g., *Romé22*'s *18.2k* simulation). A monostable, weak AMOC is not found by *Romé22*. However, other previous studies have demonstrated collapsed and unrecoverable AMOCs with high freshwater fluxes (e.g., [97]), and we can hypothesize that with higher meltwater fluxes we would have reached this regime. In this study, and previous studies such as [53], lowering atmospheric CO_2 concentration forces the AMOC along the bistability curve in the same direction as elevated freshwater (e.g., ice sheet meltwater) discharge to the oceans. Our *CO_2_210ppm* simulation represents the monostable, strong AMOC; the *CO_2_200ppm* simulation fits the profile of an excitable strong AMOC regime; the system moves into the oscillatory regime from *REF* and remains there with a CO_2 concentration of 180 ppm. This study does not include simulations with an atmospheric CO_2 concentration lower than 180 ppm, so it is uncertain whether the AMOC would move further on, eventually to a monostable, weak AMOC. However, Klockmann et al. [53] do demonstrate that this behavior can be obtained with low CO_2 simulations under pre-industrial conditions.

How the forcing of boreal seasonality (e.g., through insolation changes) moves AMOC through this bistability curve is more complex. As the strength of boreal seasonality changes, the AMOC does not move in or out of the oscillatory regime. Instead, as the boreal seasonality strength increases, the oscillations decrease in periodicity and as the *Orbit_10k* simulation demonstrates, begin to oscillate in a *warm* (i.e., interstadial) mode. However, how the periodicity is impacted (i.e., the length of time spent in a *warm*/strong AMOC phase and a *cold*/weak AMOC phase, relative to *REF*) is not purely dependent on boreal seasonality alone, but controlled by the combination of the independent orbital parameters. For instance, despite both simulations having stronger boreal seasonality, *Orbit_30k* has a longer *cold* mode than *REF* whereas *Orbit_10k* does not reenter the *cold* mode. We put this down to the differences in obliquity, which impact how the insolation is distributed across the globe, creating contrasting localized effects (i.e., the higher incoming solar radiation in the high latitudes of *Orbit_10k* than in *Orbit_30k*; Figure 1f, resulting in variations in the sea ice thickness distribution; Supplementary Figure S3) and leading to different patterns of oscillatory behavior. In conclusion, changes in orbital forcing should not be considered a simple forcing but a way to deeply modify the shape of the bifurcation diagram.

4.2. Glacial terminations and the "window of opportunity"

Barker and Knorr [64] suggest four possible scenarios for how the AMOC could recover during a glacial

termination: an increase in North American ice sheet height (producing stronger winds and thus a stronger AMOC [42,98–100]), an AMOC recovery during a bistable window from an external forcing like a negative freshwater event, an increase in CO_2 concentration that outpaces the rate of ice sheet decline, or a CO_2 increase that reaches the needed interglacial threshold. Our high CO_2 simulations demonstrate from a mechanistic perspective the validity of the latter two situations.

Because no other variables have been changed, from the *CO_2_200ppm* and *CO_2_210ppm* simulations we were able to isolate the impact of an increase in CO_2 similar to the 10 ppm rise in atmospheric CO_2 that occurs between Heinrich Stadial 1 (a cold period between ~18.5 and 14.7 ka BP characterized by weak ocean circulation [101–105]) and the Bølling-Allerød Warming (an abrupt warming ~14.7 ka BP in Greenland [106–108]). The constant ice sheet geometry in our experiments, however, is not an unreasonable approximation for the relatively slow and minor North American ice sheet evolution reconstructed between 21 and 17 ka BP [82,109]. Thus, our simulations demonstrate that an addition of only 10 ppm of CO_2 can be enough to move the AMOC from a bistable to a monostable strong regime, reaching the needed interglacial threshold. Once CO_2 levels reach a certain point, e.g., near-interglacial levels, the AMOC bifurcates to a steady interglacial state. Reversing the direction of CO_2 change, our atmospheric CO_2 experiments also show how only a small change in CO_2 concentration could move the climate from a more stable regime to within the "window of opportunity."

Moreover, we have demonstrated one way in which background climate state can condition the ocean to be more vulnerable to tipping across density thresholds, triggering and controlling the nature of unforced AMOC oscillations, but the nuances of this relationship between background climate and AMOC oscillation become clearer when we compare our results to previous work. For example, Malmierca-Vallet et al. [68] empirically identified a similar atmospheric CO_2 "window of opportunity" for AMOC oscillations in three different models under different background climates and boundary conditions: ~185 to 230 ppm. Notably, 230 ppm, the top end of their window, is higher than ours ($<$ 200 ppm). Additionally, 185 ppm, the bottom end of their window, is higher than our lowest CO_2 simulation (180 ppm), though we do not have enough simulations to identify a comprehensive range. Notwithstanding the differences in the trigger for the oscillations [50,57], the contextual differences in the experimental designs—i.e., dissimilarity in initial and boundary conditions, such as the meltwater flux in ours and the ice sheet geometry—are likely key in explaining this difference between the CO_2 threshold for oscillation in our results and the earlier work.

The impact of boundary and initial conditions on a "window of opportunity" for AMOC oscillation are clearest when comparing simulations run with the same model. For example, although our *Orbit_30k* simulation and the HadCM3 simulations presented by [68] share the same orbital forcing (from 30 ka BP), our glacial maximum ice sheets are much larger than the mid-glacial sized ice sheets [110] implemented by [68]. The larger glacial maximum ice sheets tend to produce stronger winds over the North Atlantic and thus a stronger AMOC, suppressing oscillations from being triggered at higher atmospheric pCO_2.

The important role of the background climate state in influencing the characteristics of triggered oscillations is further confirmed when comparing our *Orbit_30k* simulation with the full 30 ka BP experiment of Armstrong et al. [57], which includes the 30 ka BP orbit, 200 ppm atmospheric CO_2, and the mid-glacial "ICE-5G" ice sheet of Peltier [110]. The previously published oscillations are of similar periodicity to our *Orbit_30k* simulation, both around 1,200 years. However, the amplitudes of the oscillations differ between the two studies. The AMOC in the simulation presented by [57] ranges in maximum strength from 6 to 12 Sv, whereas the AMOC oscillations in our *Orbit_30k* run span a larger amplitude from 6 to 18 Sv. Considering that in our other simulations, as well as previous studies (e.g., [53]), AMOC strengthening correlates with higher atmospheric CO_2, it is interesting that Armstrong et al. [57]'s maximum AMOC strength is lower than ours even though their atmospheric CO_2 concentration is 10 ppm higher, suggesting that in this case, the above-described influence of ice sheet size/geometry on the AMOC overrides the smaller impact of atmospheric CO_2. The similarity in the shape and periodicity of the oscillations, despite the impact of differences in ice sheet size and CO_2 concentration on the amplitude, hints at the importance of the orbital control on insolation patterns compared to other forcings during this time period.

In our other orbit simulations, the *Orbit_10k* simulation has the strongest boreal seasonality and the *Orbit_21.5k* simulation has the weakest boreal seasonality (with *REF* only stronger by a difference of less than 1 W m^{-2} in seasonal insolation). The change in periodicity of our simulations is consistent with the findings of both [29] and [55], and for our simulations, we explain this with the changes in sea ice relative to *REF*. The *Orbit_10k* simulation displays oscillations of the shortest periodicity (only ~500 years). The *Orbit_30k* simulation, which has the second strongest boreal seasonality, has oscillations ~1,200 years in length. The *warm–cold* cycles in *REF* and *Orbit_21.5k* are ~1,500 years in length. However, unlike [29], where oscillations under high obliquity were not observed, we do find oscillations in *Orbit_10k*, the simulation with the highest obliquity—but, as a reminder, these centennial-scale oscillations are

much shorter in amplitude and less D-O-like than the other oscillatory behavior in our results, but can still be a natural mode of variability in the ocean system [111].

Previous studies, including [64] and [58], demonstrate that the combination of changes between atmospheric CO_2 and ice volume control the sensitivity of AMOC to other climate perturbations, such as orbitally induced changes in insolation. These studies have not found any AMOC mode changes under peak glacial or interglacial conditions, but they have produced AMOC oscillations under intermediate conditions (i.e., between glacial and interglacial states) with changes in orbit, atmospheric CO_2 concentration, and ice volume. Although we observe very different variations in the oscillatory behavior in our simulations, they are only tested under one background climate. It would be interesting to further test our results against other background climates.

5. Conclusion

In this study, we present six new simulations from the Hadley Centre general circulation model version 3 (HadCM3), with four of the simulations oscillating under glacial climate conditions. These simulations are sensitivity experiments branching from *Romé22*'s *20.7k* simulation with Last Glacial Maximum conditions and a constant meltwater flux derived from the GLAC-1D ice sheet reconstruction of the early deglaciation. We tested the impact of different atmospheric CO_2 concentrations and orbital forcing on the oscillations and their respective mechanisms of AMOC millennial-scale variability [83].

Our results showed that raising CO_2 concentrations from 190 to 200 and 210 ppm prevents the periodic AMOC oscillations from occurring, whereas decreasing atmospheric CO_2 to 180 ppm shortened the duration of the *warm* (or interstadial) phase, by ~200 years, and led to an overall shorter periodicity of the oscillation. In addition, we observe that when boreal seasonality increases (equivalent to conditions at 30 ka BP), the duration of the *warm*, interstadial phase decreases. However, the simulation with the strongest boreal seasonality (equivalent to conditions at 10 ka BP) remains in a relatively *warm*, interstadial state with centennial-scale AMOC oscillations between 12 and 18 Sv. We hypothesize that this contrasting response is due to differences in obliquity (with obliquity low at 30 ka BP and high at 10 ka BP) impacting sea ice thickness.

We show that the sensitivity of the mechanism for AMOC millennial-scale variability to changes in climate forcings (atmospheric CO_2 and orbital configuration) is primarily controlled by sea ice conditions. This effect is overlaid on the convection–advection mechanism described by [83], and can modify the periodicity, the amplitude and the shape of the oscillations. This is mostly due to the effect of Northern Hemisphere sea ice volume on the freshening or the thermal insulation of convection sites. We add two new branches to the convection–advection mechanism to explain the new AMOC behavior demonstrated in this study, where the AMOC skips the cold, weak phase (as was the case for 10 ka BP orbital conditions and at higher levels of CO_2) and where increased sea ice volume results in a faster transition out of the warm, strong phase (as was the case for 30 ka BP orbital conditions and at a lower CO_2 level). In either case, sea ice thickness during a particular AMOC phase can determine the salinity concentration in the GIN and Irminger seas and therefore whether the AMOC reaches a stratification threshold in the direction of weakening or strengthening. The impacts of changes in CO_2 concentration and orbital insolation forcing on our AMOC oscillations demonstrate the importance of the role of sea ice thickness in controlling the speed at which the AMOC can switch between warm and cold regimes. Furthermore, these impacts demonstrate how even small changes to the background climate condition can significantly impact the AMOC's ability to oscillate.

Acknowledgments

BS acknowledges support from their supervisors, the NERC DTP, and their co-authors in the efforts of this study.

Author contributions

CRediT: **Brooke Snoll**: Conceptualization, Data curation, Formal analysis, Investigation, Methodology, Project administration, Resources, Validation, Visualization, Writing – original draft, Writing – review & editing; **Ruza Ivanovic**: Conceptualization, Methodology, Project administration, Supervision, Writing – review & editing; **Lauren J. Gregoire**: Conceptualization, Methodology, Supervision, Writing – review & editing; **Sam Sherriff-Tadano**: Conceptualization, Methodology, Supervision, Writing – review & editing; **Yvan Romé**: Conceptualization, Resources, Writing – review & editing.

Disclosure statement

One of the coauthors is a member of the editorial board of *Critical Insights in Climate Change*. The other authors have no other competing interests to declare.

Funding

BS is supported by the Leeds–York–Hull Natural Environment Research Council (NERC) Doctoral Training Partnership (DTP) Panorama under grant NE/S007458/1.

ORCID

Brooke Snoll http://orcid.org/0000-0002-3091-4394

Data availability statement

Data is available via https://doi.org/10.5518/1624, and code is available via https://doi.org/10.5281/zenodo.17177068. The corresponding author, BS, can assist with any questions about the data or code upon reasonable request.

References

1. Armstrong McKay DI, Staal A, Abrams JF, et al. Exceeding 1.5 °C global warming could trigger multiple climate tipping points. Science. 2022;377(6611):eabn7950. doi: 10.1126/science.abn7950
2. Fletcher WJ, Sánchez Goñi MF, Allen JRM, et al. Millennial-scale variability during the Last Glacial in vegetation records from Europe. Quat Sci Rev. 2010;29(21-22):2839–2864. doi: 10.1016/j.quascirev.2009.11.015
3. Fritz SC, Baker PA, Ekdahl E, et al. Millennial-scale climate variability during the Last Glacial period in the tropical Andes. Quat Sci Rev. 2010;29(7-8):1017–1024. doi: 10.1016/j.quascirev.2010.01.001
4. Wolff EW, Chappellaz J, Blunier T, et al. Millennial-scale variability during the last glacial: the ice core record. Quat Sci Rev. 2010;29(21-22):2828–2838. doi: 10.1016/j.quascirev.2009.10.013
5. Andersen KK, Svensson A, Johnsen SJ, et al. The Greenland Ice Core Chronology 2005, 15–42 ka. Part 1: constructing the time scale. Quat Sci Rev. 2006;25(23-24):3246–3257. doi: 10.1016/j.quascirev.2006.08.002
6. Huber C, Leuenberger M, Spahni R, et al. Isotope calibrated Greenland temperature record over Marine Isotope Stage 3 and its relation to CH4. Earth Planet Sci Lett. 2006;243(3-4):504–519. doi: 10.1016/j.epsl.2006.01.002
7. Kindler P, Guillevic M, Baumgartner M, et al. Temperature reconstruction from 10 to 120 kyr b2k from the NGRIP ice core. Clim Past. 2014;10(2):887–902. doi: 10.5194/cp-10-887-2014
8. Sanchez Goñi MF, Harrison SP. Millennial-scale climate variability and vegetation changes during the Last Glacial: concepts and terminology. Quat Sci Rev. 2010;29(21-22):2823–2827. doi: 10.1016/j.quascirev.2009.11.014
9. Dansgaard W, Johnsen SJ, Clausen HB, et al. North Atlantic climatic oscillations revealed by deep Greenland ice cores. In: Hansen E, Takahashi T, editor. Climate processes and climate sensitivity. Washington, DC: American Geophysical Union (AGU); 1984. p. 288–298. doi: 10.1029/GM029p0288https://onlinelibrary.wiley.com/doi/abs/10.1029/GM029p0288
10. Johnsen SJ, Clausen HB, Dansgaard W, et al. Irregular glacial interstadials recorded in a new Greenland ice core. Nature. 1992;359(6393):311–313. doi: 10.1038/359311a0
11. North Greenland Ice Core Project Members. High-resolution record of Northern Hemisphere climate extending into the last interglacial period. Nature. 2004;431(7005):147–151. doi: 10.1038/nature02805
12. Adolphi F, Bronk Ramsey C, Erhardt T, et al. Connecting the Greenland ice-core and UTh timescales via cosmogenic radionuclides: testing the synchroneity of Dansgaard–Oeschger events. Clim Past. 2018;14(11):1755–1781. doi: 10.5194/cp-14-1755-2018
13. Deplazes G, Lückge A, Peterson LC, et al. Links between tropical rainfall and North Atlantic climate during the Last Glacial period. Nature Geosci. 2013;6(3):213–217. doi: 10.1038/ngeo1712
14. Asmerom Y, Polyak VJ, Burns SJ. Variable winter moisture in the southwestern United States linked to rapid glacial climate shifts. Nature Geosci. 2010;3(2):114–117. doi: 10.1038/ngeo754
15. Vanneste H, De Vleeschouwer F, Martínez-Cortizas A, et al. Late-glacial elevated dust deposition linked to westerly wind shifts in southern South America. Sci Rep. 2015;5(1):11670. doi: 10.1038/srep11670
16. Wang X, Auler AS, Edwards RL, et al. Wet periods in northeastern Brazil over the past 210 kyr linked to distant climate anomalies. Nature. 2004;432(7018):740–743. doi: 10.1038/nature03067
17. Rousseau D-D, Boers N, Sima A, et al. (MIS3 & 2) millennial oscillations in Greenland dust and Eurasian aeolian records – a paleosol perspective. Quat Sci Rev. 2017;169:99–113. doi: 10.1016/j.quascirev.2017.05.020
18. Wang Y, Cheng H, Edwards RL, et al. Millennial- and orbital-scale changes in the East Asian monsoon over the past 224,000 years. Nature. 2008;451(7182):1090–1093. doi: 10.1038/nature06692
19. Rahmstorf S. Ocean circulation and climate during the past 120,000 years. Nature. 2002;419(6903):207–214. doi: 10.1038/nature01090
20. Schulz M. On the 1470-year pacing of Dansgaard-Oeschger warm events. Paleoceanography. 2002;17(2):4–1–4–9. doi: 10.1029/2000PA000571
21. Böhm E, Lippold J, Gutjahr M, et al. Strong and deep Atlantic meridional overturning circulation during the Last Glacial cycle. Nature. 2015;517(7532):73–76. doi: 10.1038/nature14059
22. Henry LG, McManus JF, Curry WB, et al. North Atlantic ocean circulation and abrupt climate change during the last glaciation. Science. 2016;353(6298):470–474. doi: 10.1126/science.aaf5529
23. Malmierca-Vallet I, Sime LC, The D–O Community Members. Dansgaard–Oeschger events in climate models: review and baseline Marine Isotope Stage 3 (MIS3) protocol. Clim Past. 2023;19(5):915–942. doi: 10.5194/cp-19-915-2023
24. Menviel LC, Skinner LC, Tarasov L, et al. An ice–climate oscillatory framework for Dansgaard–Oeschger cycles. Nat Rev Earth Environ. 2020;1(12):677–693. doi: 10.1038/s43017-020-00106-y
25. Vettoretti G, Peltier WR. Thermohaline instability and the formation of glacial North Atlantic super polynyas at the onset of Dansgaard-Oeschger warming events. Geophys Res Lett. 2016;43(10):5336–5344. doi: 10.1002/2016GL068891
26. Vettoretti G, Peltier WR. Fast physics and slow physics in the nonlinear Dansgaard–Oeschger relaxation oscillation. J Clim. 2018;31:3423–3449. doi: 10.1175/JCLI-D-17-0559.1
27. Lynch-Stieglitz J, Adkins JF, Curry WB, et al. Atlantic meridional overturning circulation during the Last Glacial Maximum. Science. 2007;316(5821):66–69. doi: 10.1126/science.1137127
28. McCarthy G, Smeed DA, Cunningham SA, et al. Atlantic Meridonal Overturning Circulation. MCCIP Sci Rev. 2017;2017:7. doi: 10.14465/2017.ARC10.002-ATLhttp://www.mccip.org.uk/impacts-report-cards/full-report-cards/2017-10-year-report-card/climate-of-the-marine-environment/atlantic-meridional-overturning-circulation-amoc/
29. Brown N, Galbraith ED. Hosed vs. unhosed: interruptions of the Atlantic Meridional Overturning Circulation in a global coupled model, with and without freshwater forcing. Clim Past. 2016;12(8):1663–1679. doi: 10.5194/cp-12-1663-2016
30. Du Y, Brown JR, Menviel L, et al. The impacts of an AMOC slowdown on Southern Hemisphere and Australian climates at 8.2 ka in ACCESS-ESM1.5 model. JGR Atmos. 2025;130(8):e2024JD042432. https://onlinelibrary.wiley.com/doi/abs/10.1029/2024JD042432 doi: 10.1029/2024JD042432

31. Jackson LC, Wood RA. Timescales of AMOC decline in response to fresh water forcing. Clim Dyn. 2018;51(4):1333–1350. doi: 10.1007/s00382-017-3957-6
32. Ma Q, Shi X, Scholz P, et al. Revisiting climate impacts of an AMOC slowdown: dependence on freshwater locations in the North Atlantic. Sci Adv. 2024;10(47):eadr3243. doi: 10.1126/sciadv.adr3243
33. Matero ISO, Gregoire LJ, Ivanovic RF, et al. The 8.2 ka cooling event caused by Laurentide ice saddle collapse. Earth Planet Sci Lett. 2017;473:205–214. doi: 10.1016/j.epsl.2017.06.011
34. Rahmstorf S. Decadal variability of the thermohaline ocean circulation. In: Navarra A, editor. Beyond El Niño. Berlin (Germany): Springer Berlin Heidelberg; 1999. p. 309–331). doi: 10.1007/978-3-642-58369-8_15
35. Roche DM, Wiersma AP, Renssen H. A systematic study of the impact of freshwater pulses with respect to different geographical locations. Clim Dyn. 2010;34(7-8):997–1013. doi: 10.1007/s00382-009-0578-8
36. Smith RS, Gregory JM. A study of the sensitivity of ocean over-turning circulation and climate to freshwater input in different regions of the North Atlantic. Geophys Res Lett. 2009;36(15):L15701. doi: 10.1029/2009GL038607
37. Roberts WHG, Valdes PJ, Payne AJ. A new constraint on the size of Heinrich events from an iceberg/sediment model. Earth Planet Sci Lett. 2014;386:1–9. doi: 10.1016/j.epsl.2013.10.020
38. Barker S, Chen J, Gong X, et al. Icebergs not the trigger for North Atlantic cold events. Nature. 2015;520(7547):333–336. doi: 10.1038/nature14330
39. Bond GC, Lotti R. Iceberg discharges into the North Atlantic on millennial time scales during the last glaciation. Science. 1995;267(5200):1005–1010. doi: 10.1126/science.267.5200.1005
40. Gregoire LJ, Payne AJ, Valdes PJ. Deglacial rapid sea level rises caused by ice-sheet saddle collapses. Nature. 2012;487(7406):219–222. doi: 10.1038/nature11257
41. Ivanovic RF, Gregoire LJ, Burke A, et al. Acceleration of northern ice sheet melt induces AMOC slowdown and northern cooling in simulations of the early last deglaciation. Paleoceanog and Paleoclimatol. 2018;33(7):807–824. doi: 10.1029/2017PA003308
42. Kapsch M, Mikolajewicz U, Ziemen F, et al. Ocean response in transient simulations of the last deglaciation dominated by underlying ice-sheet reconstruction and method of meltwater distribution. Geophys Res Lett. 2022;49(3):e2021GL096767. doi: 10.1029/2021GL096767
43. Snoll B, Ivanovic RF, Valdes PJ, et al. Effect of orographic gravity wave drag on Northern Hemisphere climate in transient simulations of the last deglaciation. Clim Dyn. 2022;59(7-8):2067–2079. doi: 10.1007/s00382-022-06196-2
44. Hu A, Van Roekel L, Weijer W, et al. Role of AMOC in transient climate response to greenhouse gas forcing in two coupled models. J Clim. 2020;33:5845–5859. doi: 10.1175/JCLI-D-19-1027.1
45. Madan G, Gjermundsen A, Iversen SC, et al. The weakening AMOC under extreme climate change. Clim Dyn. 2024;62(2):1291–1309. doi: 10.1007/s00382-023-06957-7
46. Muthers S, Raible CC, Rozanov E, et al. Response of the AMOC to reduced solar radiation–the modulating role of atmospheric chemistry. Earth Syst Dynam. 2016;7(4):877–892. doi: 10.5194/esd-7-877-2016
47. Nobre P, Veiga SF, Giarolla E, et al. AMOC decline and recovery in a warmer climate. Sci Rep. 2023;13(1):15928. doi: 10.1038/s41598-023-43143-5
48. Toggweiler JR, Russell J. Ocean circulation in a warming climate. Nature. 2008;451(7176):286–288. doi: 10.1038/nature06590
49. Zhu J, Liu Z, Zhang J, et al. AMOC response to global warming: dependence on the background climate and response timescale. Clim Dyn. 2015;44(11-12):3449–3468. doi: 10.1007/s00382-014-2165-x
50. Romé YM, Ivanovic RF, Gregoire LJ, et al. Millennial-scale climate oscillations triggered by deglacial meltwater discharge in Last Glacial Maximum simulations. Paleoceanog Paleoclimatol. 2022;37(10):2572–4525. doi: 10.1029/2022PA004451
51. Sherriff-Tadano S, Abe-Ouchi A. Roles of sea ice–surface wind feedback in maintaining the glacial Atlantic meridional overturning circulation and climate. J Clim. 2020;33(8):3001–3018. doi: 10.1175/JCLI-D-19-0431.1
52. Drijfhout S, Gleeson E, Dijkstra HA, et al. Spontaneous abrupt climate change due to an atmospheric blocking–sea-ice–ocean feedback in an unforced climate model simulation. Proc Natl Acad Sci USA. 2013;110(49):19713–19718. doi: 10.1073/pnas.1304912110
53. Klockmann M, Mikolajewicz U, Marotzke J. Two AMOC states in response to decreasing greenhouse gas concentrations in the coupled climate model MPI-ESM. J Clim. 2018;31(19):7969–7984. doi: 10.1175/JCLI-D-17-0859.1
54. Martin T, Park W, Latif M. Southern Ocean forcing of the North Atlantic at multi-centennial time scales in the Kiel Climate Model. Deep Sea Res Part II. 2015;114:39–48. doi: 10.1016/j.dsr2.2014.01.018
55. Kuniyoshi Y, Abe-Ouchi A, Sherriff-Tadano S, et al. Effect of climatic precession on Dansgaard-Oeschger-like oscillations. Geophys Res Lett. 2022;49(6). doi: 10.1029/2021GL095695
56. Peltier WR, Vettoretti G. Dansgaard-Oeschger oscillations predicted in a comprehensive model of glacial climate: a "kicked" salt oscillator in the Atlantic. Geophys Res Lett. 2014;41(20):7306–7313. doi: 10.1002/2014GL061413
57. Armstrong E, Izumi K, Valdes P. Identifying the mechanisms of DO-scale oscillations in a GCM: a salt oscillator triggered by the Laurentide ice sheet. Clim Dyn. 2023;60(11-12):3983–4001. doi: 10.1007/s00382-022-06564-y
58. Zhang X, Barker S, Knorr G, et al. Direct astronomical influence on abrupt climate variability. Nat Geosci. 2021;14(11):819–826. doi: 10.1038/s41561-021-00846-6
59. Bitz CM, Chiang JCH, Cheng W, et al. Rates of thermohaline recovery from freshwater pulses in modern, Last Glacial Maximum, and greenhouse warming climates. Geophys Res Lett. 2007;34(7):L07708. doi: 10.1029/2006GL029237
60. Dome Fuji Ice Core Project Members, Kawamura K, Abe-Ouchi A, et al. State dependence of climatic instability over the past 720,000 years from Antarctic ice cores and climate modeling. Sci Adv. 2017;3(2):e1600446. doi: 10.1126/sciadv.1600446
61. Pöppelmeier F, Jeltsch-Thömmes A, Lippold J, et al. Multiproxy constraints on Atlantic circulation dynamics since the last ice age. Nat Geosci. 2023;16(4):349–356. doi: 10.1038/s41561-023-01140-3
62. Schmittner A, Lund DC. Carbon isotopes support Atlantic meridional overturning circulation decline as a trigger for early deglacial CO_2 rise. Clim Past Discuss. 2014;10:2857–2893. doi: 10.5194/cpd-10-2857-2014
63. Vettoretti G, Ditlevsen P, Jochum M, et al. Atmospheric CO_2 control of spontaneous millennial-scale ice age climate oscillations. Nat Geosci. 2022;15(4):300–306. doi: 10.1038/s41561-022-00920-7
64. Barker S, Knorr G. Millennial scale feedbacks determine the shape and rapidity of glacial termination. Nat Commun. 2021;12(1):2273. doi: 10.1038/s41467-021-22388-6
65. Willeit M, Ganopolski A, Edwards NR, et al. Surface buoyancy control of millennial-scale variations in the Atlantic

meridional ocean circulation. Clim Past. 2024;20(12):2719–2739. doi: 10.5194/cp-20-2719-2024
66. Zhang X, Knorr G, Lohmann G, et al. Abrupt North Atlantic circulation changes in response to gradual CO_2 forcing in a glacial climate state. Nature Geosci. 2017;10(7):518–523. doi: 10.1038/ngeo2974
67. Obase T, Abe-Ouchi A. Abrupt Bølling-Allerød warming simulated under gradual forcing of the last deglaciation. Geophys Res Lett. 2019;46(20):11397–11405. doi: 10.1029/2019GL084675
68. Malmierca-Vallet I, Sime LC, Valdes PJ, et al. The impact of CO_2 and climate state on whether Dansgaard–Oeschger type oscillations occur in climate models. Geophys Res Lett. 2024;51(13). doi: 10.1029/2024GL110068
69. Gregoire LJ, Valdes PJ, Payne AJ. The relative contribution of orbital forcing and greenhouse gases to the North American deglaciation. Geophys Res Lett. 2015;42(22):9970–9979. doi: 10.1002/2015GL066005
70. Jouzel J, Masson-Delmotte V, Cattani O, et al. Orbital and millennial Antarctic climate variability over the past 800,000 years. Science. 2007;317(5839):793–796. doi: 10.1126/science.1141038
71. Erb MP, Broccoli AJ, Clement AC. The contribution of radiative feedbacks to orbitally driven climate change. J Clim. 2013;26(16):5897–5914. doi: 10.1175/JCLI-D-12-00419.1
72. Yin QZ, Wu ZP, Berger A, et al. Insolation triggered abrupt weakening of Atlantic circulation at the end of interglacials. Science. 2021;373(6558):1035–1040. doi: 10.1126/science.abg1737
73. Li C, Battisti DS, Bitz CM. Can North Atlantic Sea Ice anomalies account for Dansgaard–Oeschger climate signals?*. J Clim. 2010;23(20):5457–5475. doi: 10.1175/2010JCLI3409.1
74. Dokken TM, Nisancioglu KH, Li C, et al. Dansgaard-Oeschger cycles: interactions between ocean and sea ice intrinsic to the Nordic seas: D-O cycles as seen in the Nordic seas. Paleoceanography. 2013;28(3):491–502. doi: 10.1002/palo.20042
75. Li C, Born A. Coupled atmosphere-ice-ocean dynamics in Dansgaard-Oeschger events. Quat Sci Rev. 2019;203:1–20. doi: 10.1016/j.quascirev.2018.10.031
76. Sadatzki H, Maffezzoli N, Dokken TM, et al. Rapid reductions and millennial-scale variability in Nordic Seas sea ice cover during abrupt glacial climate changes. Proc Natl Acad Sci USA. 2020;117(47):29478–29486. doi: 10.1073/pnas.2005849117
77. Cheng W, Weijer W, Kim WM, et al. Can the salt-advection feedback be detected in internal variability of the Atlantic meridional overturning circulation? Journal of Climate. 2018;31(16):6649–6667. doi: 10.1175/JCLI-D-17-0825.1
78. Kageyama M, Albani S, Braconnot P, et al. The PMIP4 contribution to CMIP6 – part 4: scientific objectives and experimental design of the PMIP4-CMIP6 Last Glacial Maximum experiments and PMIP4 sensitivity experiments. Geosci Model Dev. 2017;10(11):4035–4055. doi: 10.5194/gmd-10-4035-2017
79. Briggs RD, Pollard D, Tarasov L. A data-constrained large ensemble analysis of Antarctic evolution since the Eemian. Quat Sci Rev. 2014;103:91–115. doi: 10.1016/j.quascirev.2014.09.003
80. Ivanovic RF, Gregoire LJ, Kageyama M, et al. Transient climate simulations of the deglaciation 21–9 thousand years beforepresent (version 1) – PMIP4 Core experiment design and boundary conditions. Geosci Model Dev. 2016;9(7):2563–2587. doi: 10.5194/gmd-9-2563-2016
81. Tarasov L, Peltier WR. Greenland glacial history and local geodynamic consequences. Geophys J Int. 2002;150(1):198–229. doi: 10.1046/j.1365-246X.2002.01702.x
82. Tarasov L, Dyke AS, Neal RM, et al. A data-calibrated distribution of deglacial chronologies for the North American ice complex from glaciological modeling. Earth Planet Sci Lett. 2012;315-316:30–40. doi: 10.1016/j.epsl.2011.09.010
83. Romé YM, Ivanovic RF, Gregoire LJ, et al. Simulated millennial-scale climate variability driven by a convection–advection oscillator. Clim Dyn. 2025;63(3):150. doi: 10.1007/s00382-025-07630-x
84. Gordon C, Cooper C, Senior CA, et al. The simulation of SST, sea ice extents and ocean heat transports in a version of the Hadley Centre coupled model without flux adjustments. Clim Dyn. 2000;16(2-3):147–168. doi: 10.1007/s003820050010
85. Pope VD, Gallani ML, Rowntree PR, et al. The impact of new physical parametrizations in the Hadley Centre climate model: HadAM3. Clim Dyn. 2000;16(2-3):123–146. doi: 10.1007/s003820050009
86. Valdes PJ, Armstrong E, Badger MPS, et al. The BRIDGE HadCM3 family of climate models: HadCM3@Bristol v1.0. Geosci Model Dev. 2017;10(10):3715–3743. doi: 10.5194/gmd-10-3715-2017
87. Davies-Barnard T, Ridgwell A, Singarayer J, et al. Quantifying the influence of the terrestrial biosphere on glacial–interglacial climate dynamics. Clim Past. 2017;13(10):1381–1401. doi: 10.5194/cp-13-1381-2017
88. Berger A. Long-term variations of daily insolation and quaternary climatic changes. J Atmos Sci. 1978;35(12):2362–2367. doi: 10.1175/1520-0469(1978)035<2362:LTVODI>2.0.CO;2
89. Köhler P, Nehrbass-Ahles C, Schmitt J, et al. A 156 kyr smoothed history of the atmospheric greenhouse gases CO_2, CH_4, and N_2O and their radiative forcing. Earth Syst Sci Data. 2017;9(1):363–387. doi: 10.5194/essd-9-363-2017
90. Sherriff-Tadano S, Abe-Ouchi A, Yoshimori M, et al. Southern ocean surface temperatures and cloud biases in climate models connected to the representation of glacial deep ocean circulation. J Clim. 2023;36(11):3849–3866. doi: 10.1175/JCLI-D-22-0221.1
91. Gao Y, Liu J, Wen Q, et al. The influence of increased CO_2 concentrations on AMOC interdecadal variability under the LGM background. J Geophys Res Atmos. 2024;129(3):e2023JD039976. doi: 10.1029/2023JD039976
92. Morrill C, Anderson DM, Bauer BA, et al. Proxy benchmarks for intercomparison of 8.2 ka simulations. Clim Past. 2013;9(1):423–432. doi: 10.5194/cp9-423-2013
93. Thomas ER, Wolff EW, Mulvaney R, et al. The 8.2ka event from Greenland ice cores. Quat Sci Rev. 2007;26(1-2):70–81. doi: 10.1016/j.quascirev.2006.07.017
94. Turney CSM, Thomas ZA, Hutchinson DK, et al. Obliquity-driven expansion of North Atlantic sea ice during the last glacial. Geophys Res Lett. 2015;42(23):10,382–10,390. doi: 10.1002/2015GL066344
95. Rahmstorf S. The thermohaline ocean circulation: a system with dangerous thresholds?. Clim Change. 2000;46(3):247–256. doi: 10.1023/A:1005648404783
96. Berk J V D, Drijfhout S, Hazeleger W. Characterisation of Atlantic meridional overturning hysteresis using Langevin dynamics. Earth Syst Dynam. 2021;12(1):69–81. doi: 10.5194/esd-12-69-2021
97. Bouttes N, Lhardy F, Quiquet A, et al. Deglacial climate changes as forced by different ice sheet reconstructions. Clim Past. 2023;19(5):1027–1042. doi: 10.5194/cp-19-1027-2023
98. Löfverström M, Lora JM. Abrupt regime shifts in the North Atlantic atmospheric circulation over the last deglaciation. Geophys Res Lett. 2017;44(15):8047–8055. doi: 10.1002/2017GL074274

99. Sherriff-Tadano S, Abe-Ouchi A, Yoshimori M, et al. Influence of glacial ice sheets on the Atlantic meridional over-turning circulation through surface wind change. Clim Dyn. 2018; 50(7-8):2881–2903. doi: 10.1007/s00382-017-3780-0
100. Ullman DJ, LeGrande AN, Carlson AE, et al. Assessing the impact of Laurentide Ice Sheet topography on glacial climate. Clim Past. 2014;10(2):487–507. doi: 10.5194/cp-10-487-2014
101. Broecker W, Putnam AE. How did the hydrologic cycle respond to the two-phase mystery interval?. Quat Sci Rev. 2012;57:17–25. doi: 10.1016/j.quascirev.2012.09.024
102. Crivellari S, Chiessi CM, Kuhnert H, et al. Increased Amazon freshwater discharge during late Heinrich Stadial 1. Quat Sci Rev. 2018;181:144–155. doi: 10.1016/j.quascirev.2017.12.005
103. Huang J, Wan S, Li A, et al. Two-phase structure of tropical hydroclimate during Heinrich Stadial 1 and its global implications. Quat Sci Rev. 2019;222:105900. doi: 10.1016/j.quascirev.2019.105900
104. Huang K-F, Oppo DW, Curry WB. Decreased influence of Antarctic intermediate water in the tropical Atlantic during North Atlantic cold events. Earth Planet Sci Lett. 2014;389: 200–208. doi: 10.1016/j.epsl.2013.12.037
105. Ng HC, Robinson LF, McManus JF, et al. Coherent deglacial changes in western Atlantic Ocean circulation. Nat Commun. 2018;9(1):2947. doi: 10.1038/s41467-018-05312-3
106. Buizert C, Keisling BA, Box JE, et al. Greenland-wide seasonal temperatures during the last deglaciation. Geophys Res Lett. 2018;45(4):1905–1914. doi: 10.1002/2017GL075601
107. Lea DW, Pak DK, Peterson LC, et al. Synchroneity of tropical and high-latitude atlantic temperatures over the last glacial termination. Science. 2003;301(5638):1361–1364. doi: 10.1126/science.1088470
108. Severinghaus JP, Brook EJ. Abrupt climate change at the end of the Last Glacial period inferred from trapped air in polar ice. Science. 1999;286(5441):930–934. doi: 10.1126/science.286.5441.930
109. Peltier WR, Argus DF, Drummond R. Space geodesy constrains ice age terminal deglaciation: the global ICE-6G C (VM5a) model. JGR Solid Earth. 2015;120(1):450–487. doi: 10.1002/2014JB011176
110. Peltier WR. Global glacial isostasy and the surface of the ice-age Earth: the ICE-5G (VM2) model and GRACE. Annu Rev Earth Planet Sci. 2004;32(1):111–149. doi: 10.1146/annurev.earth.32.082503.144359
111. Sévellec F, Huck T, de Verdière AC. From centennial to millennial oscillation of the thermohaline circulation. J Mar Res. 2010;68(5):723–742. doi: 10.1357/002224011795977635